



Extending the Hong-Ou-Mandel effect: The power of nonclassicalityPaul M. Alsing ^{1,*}, Richard J. Birrittella,¹ Christopher C. Gerry,² Jihane Mimih,³ and Peter L. Knight ⁴¹*Air Force Research Laboratory, Information Directorate, 525 Brooks Road, Rome, New York 13411, USA*²*Department of Physics and Astronomy, City University of New York, Bronx, New York 10468-1589, USA*³*Department of Electrical and Computer Engineering, Naval Postgraduate School, 1 University Circle, Monterey, California 93943, USA*⁴*Blackett Laboratory, Imperial College, London SW7 2AZ, United Kingdom*

(Received 26 September 2021; revised 22 November 2021; accepted 16 December 2021; published 14 January 2022)

We show that the parity (evenness or oddness) of a nonclassical state of light has a dominant influence on the interference effects at a balanced beam splitter, irrespective of the state initially occupying the other input mode. Specifically, the parity of the nonclassical state gives rise to destructive interference effects that result in deep valleys in the output joint number distribution of which the Hong-Ou-Mandel (HOM) effect is a limiting case. The counterintuitive influence of even a single photon to control the output of a beam splitter illuminated by any field, be it a coherent or even a noisy thermal field, demonstrates the extraordinary power of nonclassicality. The canonical example of total destructive interference of quantum amplitudes leading to the absence of coincidence counts from a 50:50 beam splitter (BS) is the celebrated HOM effect, characterized by the vanishing of the joint probability of detecting single photons in each of the output beams. We show that this is a limiting case of more general input states upon which a 50:50 BS can create total, or near total, destructive interference of quantum amplitudes. For the case of an odd photon-number input Fock state of arbitrary value $n > 0$ we show that the joint photon-number probabilities vanish when detecting identical photon numbers in each output beams. We specifically examine the mixing of photon-number states of $n = 1, 2,$ and 3 with a continuous-variable state, such as a coherent state of arbitrary amplitude, and a thermal state. These vanishing joint probabilities form what we call a central nodal line: A contiguous set of zeros representing complete destructive interference of quantum amplitudes. We further show that with odd or even photon-number Fock states n , with $n > 1$, there will be additional off-diagonal curves along which the joint photon-number probabilities are either zero, or near zero, which we call pseudonodal curves, which constitute a near, but not complete, destructive interference pattern in the photon-number space. We interpret all of these interference effects as an extension of the HOM effect. We explain the origin of these effects and explore the experimental prospects for observing them with currently available number-resolving detectors in the presence of a small amount of noise.

DOI: [10.1103/PhysRevA.105.013712](https://doi.org/10.1103/PhysRevA.105.013712)**I. INTRODUCTION**

The generation of two-mode entangled states of light can be accomplished by mixing nonclassical single-mode states of light at a beam splitter (BS) [1]. The process that gives rise to such two-mode states of light via beam splitting is known as multiphoton interference [2] and serves as a critical element in several applications including quantum optical interferometry [3] and quantum state engineering where beam splitters and conditional measurements are utilized to perform postselection techniques such as photon subtraction [4–6], photon addition [7], and photon catalysis [8–10].

In spite of its name, multiphoton interference does not involve the interference of photons. Rather, as has been emphasized by Glauber [11], it is always the addition of the quantum amplitudes (themselves being complex numbers) associated with these states that gives rise to interference effects. The amplitudes to be added are those associated with different paths (or processes) to obtain a given final output state. Thus, the term multiphoton interference must be understood to mean interference with states containing numerous

photons. The canonical example of this kind of interference is what has come to be known as the Hong-Ou-Mandel (HOM) effect [12], which is a two-photon interference effect wherein single photons in either of the output beams of a 50:50 beam splitter emerge together (probabilistically). Detectors placed at each of the output ports will yield no simultaneous coincident clicks. That is, the input state $|1, 1\rangle_{ab}$ results in the output state $\frac{1}{\sqrt{2}}(|2, 0\rangle_{ab} + |2, 0\rangle_{ab})$. The absence of $|1, 1\rangle_{ab}$ in the output is due to the complete destructive interference between the quantum amplitudes of the two processes (both photons transmitted or both reflected) that potentially would lead to the state being in the output. The essence of this effect from an experimental point of view is that the joint probability $P_{ab}(1, 1)$ for detecting one photon in each of the output beams vanishes, i.e., $P_{ab}(1, 1) = 0$.

In this paper we show that the same complete destructive interference demonstrated by the HOM effect persists for more generalized input states such that the joint probability of measuring equal numbers of photons at the output ports of a 50:50 BS vanishes. These situations arise from the mixing of a one-photon (Fock state) and a continuous-variable (CV) state at the BS. That is, the input states could be $|\Psi\rangle_{ab} = |1\rangle_a |\psi\rangle_b$ or $\rho_{ab} = |1\rangle_a \langle 1| \otimes \rho_b$, where $|\psi\rangle_b$ and ρ_b are CV pure and

*Corresponding author: paul.alsing@us.af.mil

mixed states, respectively. For these situations we find that for a 50:50 BS the output probabilities $P_{ab}(m', m') = 0$ for all integers $m' \in \mathbb{Z}_{\geq 0}$. This means we obtain a central nodal line (CNL), or a line of zeros representing complete destructive interference, along the diagonal of the output joint photon-number distribution. We can understand this CNL [i.e., that $P_{ab}(m', m') = 0$] to be a higher-order form of the HOM effect. We further show that the mixing of odd-photon-number states with CV states, of the composite form $|n\rangle_a \langle n| \otimes \rho_b$ with odd $n \in \mathbb{Z}_{\geq 0}^{\text{odd}}$, results in a CNL $P_{ab}(m', m') = 0$ for arbitrary states ρ_b .

The Hong-Ou-Mandel effect is often characterized (e.g., observed experimentally) by the dip in the rate of coincident single-photon detections as a function of the position of the beam splitter (or, equivalently, the difference in the arrival times of the two single photons at the BS). We take the position that the whole of the dip is not, in and of itself, the central feature of the HOM effect. Rather, the HOM effect is the quantum amplitude interference effect that occurs when two photons enter a beam splitter simultaneously from opposite sides. The dip in the curve is the result of what needs to be performed experimentally to prepare and verify the required input state $|1, 1\rangle_{ab}$. In the HOM experiment, the two photons involved originate from the same source and adjusting the position of the beam splitter is required to ensure that the photons arrive there simultaneously. The HOM effect is the complete destructive interference between two photons simultaneously arriving (zero time delay) at opposite sides of a 50:50 BS, as opposed to it being the whole HOM dip (e.g., a scan across the difference in arrival times between the two photons). In short, we distinguish the HOM effect as the center (theoretical minimum) of the experimental dip, that is, the point at which the output amplitude for coincident counts vanishes due to complete destructive quantum interference.

In the case of mixing a single photon with coherent light at a beam splitter, the photons involved are from independent sources. Furthermore, the coherent state is a CV state obtained from a phase-stabilized laser continuously being shone upon the BS. The single (signal) photon will be known to have arrived at the BS by the heralding of its (idler) twin from a spontaneous parametric down-converter. Thus, the mixing of the single photon with a coherent light beam will result in multiphoton interference in bursts conditioned by the heralding of the (signal) photon. Therefore, there will be no manifestation of an HOM dip in experiments of the type envisioned here. The canonical ($|1, 1\rangle_{ab}$ input state) HOM dip occurs because there is no single-photon continuous-variable state that could be prepared and continuously shone upon a BS. It is the quantum amplitude interference effects themselves that are extensions of the HOM effect. In addition to the diagonal CNL of zeros, for any $n > 1$, even or odd, there exist sets of noncontiguous nondiagonal zeros lying on what we term pseudonodal curves (PNCs), or near-nodal curves, of the output joint probabilities that lie symmetrically placed about the diagonal. In the case of $n = 2$ there are two nondiagonal PNCs and no CNLs, while for $n = 3$ there are two nondiagonal PNCs that lie symmetrically placed on either side of the diagonal CNL. The more photons we mix on the BS, the more PNCs we obtain. In fact, the mixing of the n -photon Fock state (FS) with a CV state or a thermal state (TS) at a 50:50 BS results in the gener-

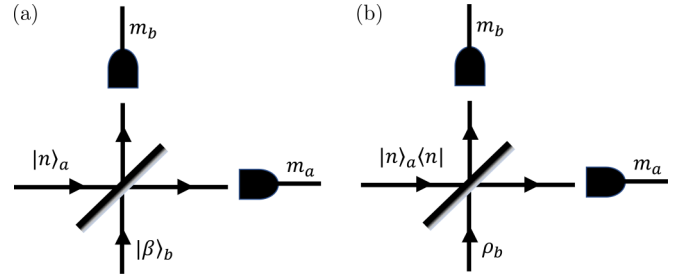


FIG. 1. Measurement of m_a and m_b photons in the output ports of a BS of transmissivity $T = \cos^2(\theta/2)$ with input Fock state $|n\rangle_a$ and (a) coherent state $|\beta\rangle_b$ and (b) thermal state ρ_b^{thermal} .

ation of n PNCs or CNLs (i.e., n nondiagonal PNCs for n even and $n - 1$ PNCs for n odd, with the addition of one diagonal CNL). The effect of the PNCs is to furcate (i.e., multiply divide) the output joint probability distribution into $n + 1$ peaks with n valleys. While these valleys are not true nodal curves, they do appear as minima in the output joint probability distribution since actual collections of (noncontiguous) zeros lie along these PNCs. All of these generalized quantum interference effects, the CNLs and the PNCs, are what we refer to as the extended HOM effect. An important point to mention here is that these effects (CNLs and PNCs) are independent of the level of excitation of the CV states. In fact, these effects are fundamental intrinsic properties of the BS itself, particularly when used in a 50:50 configuration, when acting upon discrete nonclassical (Fock) states (hence states built up from these component states). Specifically, the appearance of the CNLs and PNCs is independent of the amplitudes that describe the a - and b -mode input states, as long as there are only odd-numbered FSs entering the a mode, i.e., as long as one of the states entering the BS is a state of odd-parity [13,14], a definitively nonclassical state. The above effects involving a CV state, specifically a coherent state (CS) mixed with an n -photon FS on a 50:50 BS [Fig. 1(a)], were reported by Birrittella, Mimih and Gerry (BMG) [15] and are shown in the left columns of Figs. 2 and 3. The FS-CS case investigated by BMG illustrates the above CNL and PNC features for the case of $n = 1, 2, 3$ and serves as an archetypal example. The right columns of Figs. 2 and 3 illustrate the analogous CNLs and PNCs for the situation of a FS-TS input to a 50:50 BS as illustrated in Fig. 1(b). The similarity of the two cases illustrated in Figs. 2 and 3 is readily apparent and exemplifies the universal behavior of the CNLs and PNCs as interference patterns in the space of photon numbers arising from the 50:50 BS. The focus of BMG was devoted to quantum interferometry, and the CNL and PNC effects were not fully explored in that work. The goal of the present work is to fully explore these effects both analytically and numerically for general states and place them in the context of previous work on multiphoton interference effects. As mentioned previously, the HOM effect [12] was the first discovered effect of this type in the laboratory, although there were hints of such an effect in the theoretical work by other workers at around the same time. The history of the HOM effect and many of its ramifications has recently been reviewed by Bouchard *et al.* [16].

Ou [17] studied the multiphoton interference obtained by a single photon mixing with an n -photon-number state at a

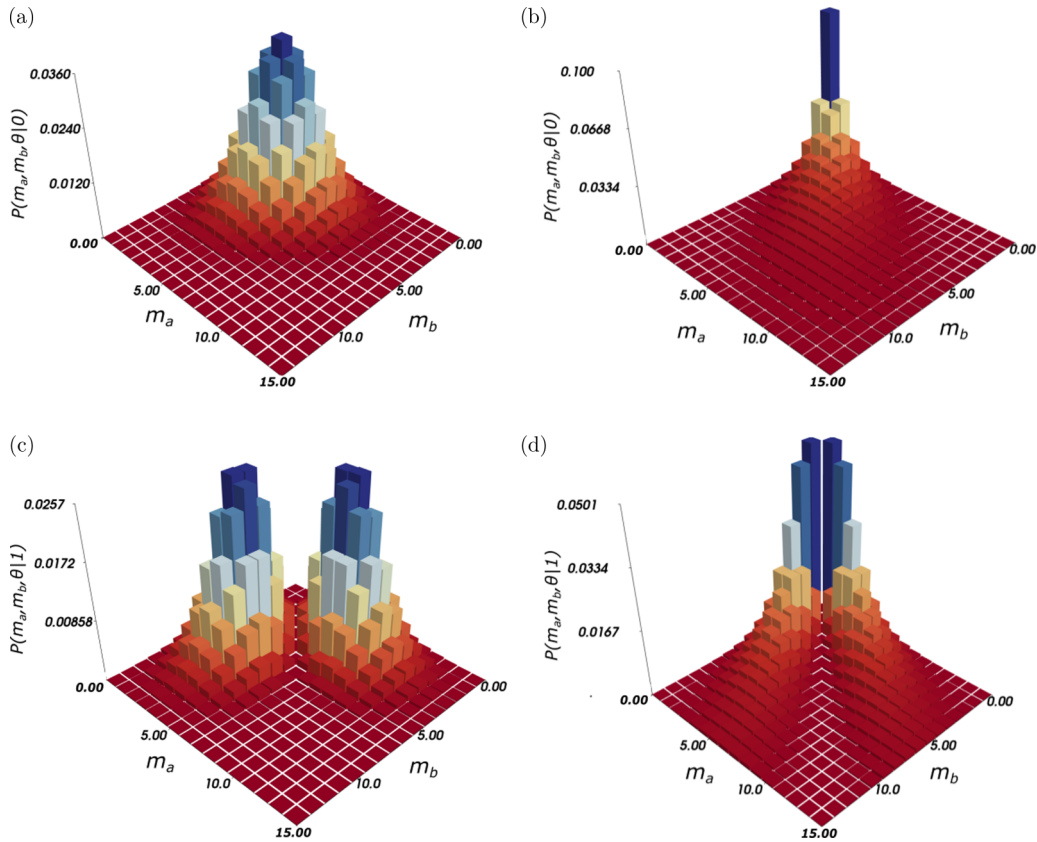


FIG. 2. Diagonal central nodal line and off-diagonal pseudonodal curves for output probability $P(m_a, m_b|n)$ for (a) and (b) $n = 0$ and (c) and (d) $n = 1$, for measurement of m_a and m_b photons at the output ports of a 50:50 BS for input Fock state $|n\rangle_a$, and (a) and (c) coherent state $|\beta\rangle_b$ with average photon number $\bar{n} = 9$ and (b) and (d) thermal state ρ_b^{thermal} with average photon number $\bar{n} = 9$, as depicted in Fig. 1.

50:50 beam splitter, where it was shown that a strong destructive interference effect was manifested in the photon-number distribution in the output. For an n -photon-number state mixing with the vacuum, the joint photon-number distribution of the output state is a two-mode binomial. With the mixing of one photon with the n -photon state one finds, if n is odd, that the joint probability for detecting $(n+1)/2$ photons in each mode is zero, i.e., $P_{ab}((n+1)/2, (n+1)/2) = 0$, as a consequence of quantum interference. However, if n is even, the combinatorics of mixing with one photon simply does not allow for output states with equal photon numbers in each mode to yield $P_{ab}(m, m) = 0$ for all m for those cases. In the same paper, Ou studied the mixing of a single photon with coherent light and with thermal light at a 50:50 beam splitter and noted that similar interference effects could be observed by balanced homodyne detection. Subsequently, Kuzmich *et al.* [18] demonstrated this effect in the laboratory for coherent light mixing with a single photon. Ou [17] and Kuzmich *et al.* [18] studied only the case where one photon is mixed with a CV state at a beam splitter. Though they noted the important interference effects, they did not explicitly describe the existence of a nodal line of zeros representing complete destructive interference in the joint photon-number distribution for the output fields, as was done by BMG [8]. Furthermore, the former authors did not extend their consideration to mixing CV states of light with two or more photons, as was done by BMG [15]. Rarity *et al.* [19] experimentally explored the HOM effect for the mixing of a single-photon state

with a separate weak coherent state and showed (via the HOM dip procedure; see their Fig. 4 in [12]) that the probability of observing one photon in each beam-splitter output approaches zero (at the minimum of the dip) due to destructive interference. Recently, Podoshvedov and An [20] have proposed the generation of even-odd CV states by quantum interference of CV states with a delocalized photon (occupying two different spatial modes) on a beam splitter. The emphasis of their work was on the entanglement properties of such generated states, as opposed to interference effects as discussed in this work. The paper that we have found that comes closest to the spirit of this present work is that of Lai, Bužek, and Knight (LBK) [21] which looked at the BS transformation on dual FS inputs to a fiber-coupler BS, including scattering losses (due to sidewall roughness). The authors reported the following: “If the same number state enters both ports of the coupler, the probability of finding an odd number of photons at either of the output ports vanishes for a particular choice of the coupler length.” The authors did not explicitly mention that this length is the one appropriate for a 50:50 fiber-coupler BS, which is most certainly the case. Additionally, the authors also considered a FS-CS input including fiber losses, but were primarily concerned with this case being a generator of displaced FS states, with the coupler behaving essentially as a homodyne detector. The inclusion of photon loss was obtained by averaging the joint photon-number distribution over a Bernoulli distribution with a Beer’s law loss parameter given by $\nu = e^{-2\gamma L}$, resulting again in marginal distributions remaining binomial

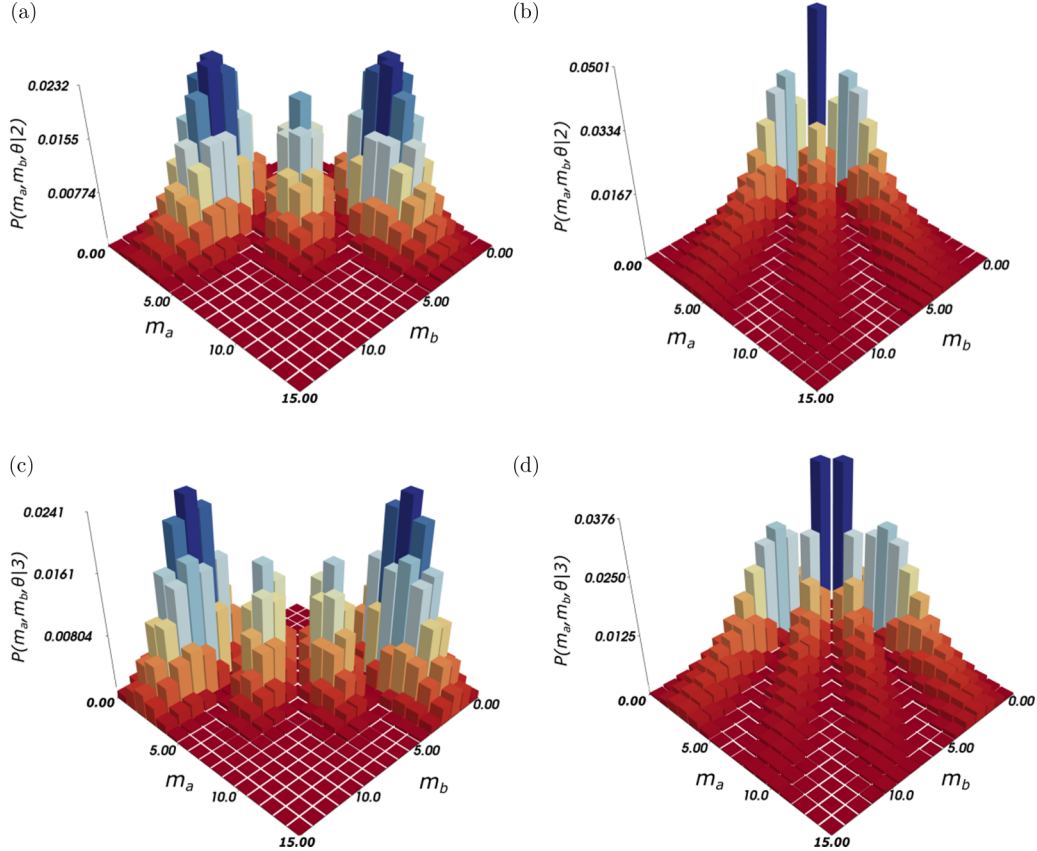


FIG. 3. Same as Fig. 2 [(a) and (c) CS and (b) and (d) TS], but now with (a) and (b) $n = 2$ and (c) and (d) $n = 3$.

in the presence of dissipation. Since the inclusion of loss is essentially straightforward, following LBK [21] [see Eqs. (41)–(43) therein] and recently Laiho *et al.* [22], we will ignore dissipation in the main exposition of this work and consider only an ideal lossless BS. The reason for this is so that we can concentrate on the universality of the CNL and PNC features discussed in this work. In a later section we show plots of the output joint photon-number distribution from the BS with loss included. In addition, with today's advances in number-resolving photon detectors (discussed in the penultimate section), photon numbers up to 5–6 can be reliably distinguished experimentally [and at some wavelengths, up to 10–20 (see [23,24])]. We will return to these considerations at the end of this work. This paper is organized as follows. In Sec. II we derive our main results concerning the CNL and PNC for a general input state and a BS with an arbitrary transmission $T = \cos^2(\theta/2)$ and reflection coefficient $R = \sin^2(\theta/2)$. Based solely on the properties of the BS rotation coefficients, we derive the general condition for the appearance of the CNL and PNC for a -mode input states containing only an odd-numbered (nonclassical) FS. In Sec. IV A we specialize to the important case of a 50:50 BS ($\theta = \pi/2$) and explore the PNC in general, as well as for the specific case considered by BMG of a FS-CS input state $|n\rangle_a|\beta\rangle_b$ with $n \in \{2, 3\}$ and an arbitrary CS of mean photon number $\bar{n}_b = |\beta|^2$. We present analytic formulas for the zeros of the PNC. We present illustrative cases for various odd-parity a -mode input states including an odd FS, photon-added single-mode squeezed state, and an odd (CS-based) cat state mixing on a

50:50 BS with a b -mode CS $|\beta\rangle_b$. Additionally, we investigate the case of a non-50:50 BS $\theta = \pi/3$ and explore the existence of analytic solutions for the PNC of the BMG scenario of a FS-CS input state $|n\rangle_a|\beta\rangle_b$ with $n \in \{2, 3\}$ mixing with a CS. In Sec. V we discuss the possible experimental realization of these effects in light of current photon-number-resolving transition edge sensors in the presence of a small amount of noise. We show plots of the output joint photon-number distribution from the BS with and without loss. Finally, in Sec. VI we conclude and discuss our general results. In Appendix A we provide the details of the derivation of the specific form of the beam-splitter coefficients upon which our main results rely. In Appendix B we provide the proof of a crucial property of the beam-splitter coefficients that is central to the appearance of the CNL. Appendix C provides tables of analytic results for zeros indicating complete destructive interference in the case of a non-50:50 beam splitter. In Appendix D we discuss the extended HOM effect and the analog of the CNL for a collection of atoms (Dicke states) using the Schwinger representation of $\text{su}(2)$ in terms of pseudo-angular-momentum states formed from two bosonic modes.

II. GENERAL CONSIDERATIONS

The HOM effect [12] is the textbook example [25,26] of the destructive interference of quantum amplitudes at a BS. We choose the convention for the BS unitary transformation (see Appendix A) with transmission coefficient

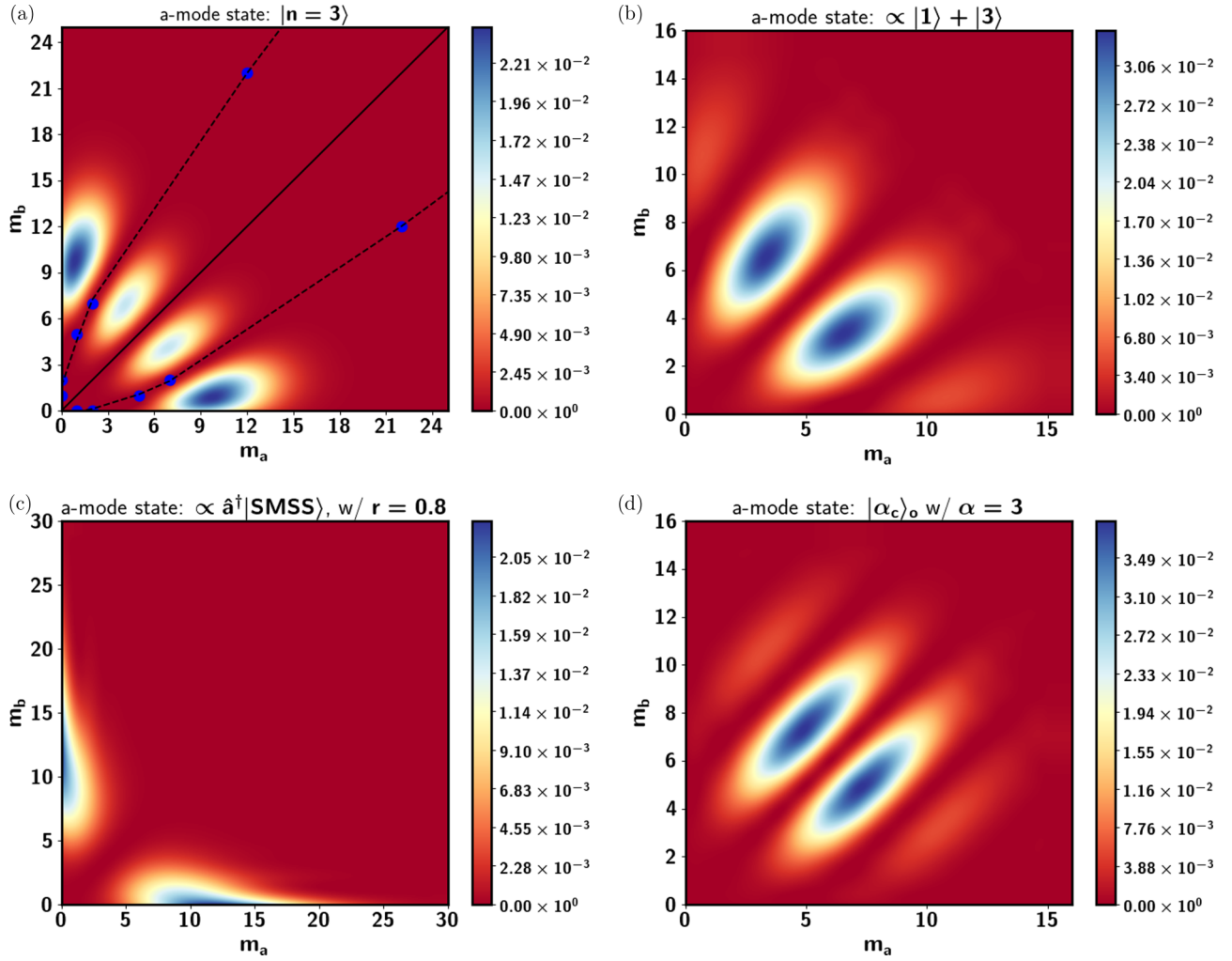


FIG. 4. Contour plots of the output joint probability $P(m_a, m_b, \theta = \pi/2)$ for a coherent state $|\beta = 3\rangle_b$ entering mode b of a 50:50 BS and a -mode input states containing only odd numbers of photons: (a) $|3\rangle_a$, (b) $(|1\rangle_a + |3\rangle_a)/\sqrt{2}$, (c) photon-added single-mode squeezed state $a^\dagger|\text{SMSS}\rangle_a$, and (d) odd cat state $|\alpha_c\rangle_a = \mathcal{N}^{-1}(|\alpha\rangle_a - |-\alpha\rangle_a)$, all showing a central nodal line along the diagonal $m_a = m_b$. The black lines and blue dots in (a) for $n = 3$ are explained in the text. (Note that all contour plots in this work are constructed by interpolating discrete data sets as displayed in the histogram plots of Figs. 2 and 3.)

$T = \cos^2(\theta/2)$ as (see Fig. 13)

$$\bar{a}^\dagger(\theta) = \begin{bmatrix} a^\dagger(\theta) \\ b^\dagger(\theta) \end{bmatrix} \equiv U(\theta) \begin{bmatrix} a^\dagger \\ b^\dagger \end{bmatrix} U^\dagger(\theta) = \begin{bmatrix} \cos(\theta/2) & \sin(\theta/2) \\ -\sin(\theta/2) & \cos(\theta/2) \end{bmatrix} \begin{bmatrix} a^\dagger \\ b^\dagger \end{bmatrix} \equiv S_{\text{BS}}(\theta) \bar{a}^\dagger \quad (1)$$

for $0 \leq \theta \leq \pi$ such that a 50:50 BS is given by $\theta = \pi/2$ ($T = R = 1/2$). Consider two single-mode FSs $|\Psi_{\text{in}}\rangle_{ab} = |1\rangle_a |1\rangle_b = a^\dagger b^\dagger |0, 0\rangle_{ab}$ entering the BS. The well-known transformation proceeds as

$$\begin{aligned} |\Psi_{\text{out}}\rangle_{ab} &= U(\theta) a^\dagger b^\dagger |0, 0\rangle_{ab} = a^\dagger(\theta) b^\dagger(\theta) |0, 0\rangle_{ab} = [a^\dagger \cos(\theta/2) + b^\dagger \sin(\theta/2)] [b^\dagger \cos(\theta/2) - a^\dagger \sin(\theta/2)] |0, 0\rangle_{ab} \\ &= \left[\frac{1}{\sqrt{2}} \left(-\frac{(a^\dagger)^2}{\sqrt{2}} + \frac{(b^\dagger)^2}{\sqrt{2}} \right) \sin(\theta) + a^\dagger b^\dagger \cos(\theta) \right] |0, 0\rangle_{ab} \xrightarrow{\theta \rightarrow \pi/2} \frac{1}{\sqrt{2}} (-|2, 0\rangle_{ab} + |0, 2\rangle_{ab}), \end{aligned} \quad (2)$$

where the minus sign in front of $|2, 0\rangle_{ab}$ arises from our choice of the BS transformation (1) and could be removed by a trivial change in phase accomplished by $a^\dagger \rightarrow ia^\dagger$ (see [25], Chap. 5). The interference of the amplitudes indicated by the $\cos(\theta)$ in front of $|1, 1\rangle_{ab}$ arises of course from the destructive interference of the two possible paths to obtain the coincident measurement $P_{ab}(1, 1) = \cos^2(\theta)$, i.e., the a and b mode are either both transmitted or both reflected into separate detectors, with equal amplitude magnitudes $\cos^2(\theta/2) = \sin^2(\theta/2) \xrightarrow{\theta \rightarrow \pi/2} = 1/2$, though opposite in sign, for a 50:50 BS. In general, since

any two-mode state (pure or mixed) can be expanded in a dual FS number basis $|n, m\rangle_{ab}$, we need to know how each basis state transforms under the action of the BS. As shown in Appendix A 3 (see also [25], Chap. 5, and [21]), we have

$$|n, m_{ab}^{(\text{out})}\rangle = U(\theta)|n, m\rangle_{ab} = \sum_{p=0}^{n+m} f_p^{(n,m)}(\theta)|p\rangle_a |n+m-p\rangle_b, \quad (3a)$$

$$f_p^{(n,m)}(\theta) = \sum_{q=0}^n \sum_{q'=0}^m \delta_{p,q+q'} \binom{n}{q} \binom{m}{q'} \sqrt{\frac{p!(n+m-p)!}{n!m!}} (-1)^{q'} [\cos(\theta/2)]^{m+(q-q')} [\sin(\theta/2)]^{n-(q-q')}. \quad (3b)$$

In Appendix A we show that through clever use of the lower factorial function $(x)_k \equiv (x-0)(x-1)(x-2)\cdots[x-(k-1)] = \frac{x!}{(x-k)!}$ [27] we can rewrite Eq. (3b) in the compact form [see (A7a) and (A7b)]

$$f_p^{(n,m)}(\theta) \equiv \frac{(-1)^{p+n}}{\sqrt{n!(m+n)_n}} \sqrt{\binom{m+n}{p}} [\cos(\theta/2)]^{m-p} [\sin(\theta/2)]^{p-n} g_p^{(n,m)}(\theta), \quad (4a)$$

where we have defined the quantity $g_p^{(n,m)}(\theta)$ as

$$g_p^{(n,m)}(\theta) \equiv \sum_{q=0}^n \binom{n}{q} (-1)^q (p)_{n-q} [\cos(\theta/2)]^{n-q} (m+n-p)_q [\sin(\theta/2)]^q, \quad (4b)$$

which will play a central role throughout this paper. Of primary interest will be the probability amplitude $\mathcal{A}(m_a, m_b, \theta|n, m)$ for the measurement (projection) $M_{ab} \equiv |m_a, m_b\rangle_{ab} \langle m_a, m_b|$ of m_a photons in mode a and m_b photons in mode b given by

$$A(m_a, m_b, \theta|n, m) = {}_{ab} \langle m_a, m_b | n, m \rangle_{ab}^{(\text{out})} = f_{m_a}^{(n, m_a+m_b-n)}(\theta) \delta_{m, m_a+m_b-n}. \quad (5)$$

The delta function δ_{m+n, m_a+m_b} ensures that one can only measure output states $|m_a, m_b\rangle$ exiting the BS such that the output sum $m_a + m_b$ is equal to the total number of photons $n + m$ entering the BS. The particular machinations that we have made in Eq. (4b) were in anticipation of the measurement M_{ab} that induces $p \rightarrow m_a$ and $m+n-p \rightarrow (m_a+m_b-n) + n - m_a = m_b$, as given by the δ function in Eq. (5). It is therefore useful to rewrite Eqs. (4a) and (4b) (apropos just after the BS, but before measurement) one final time for indices representing measurement of the output joint probability distribution of the BS. We then explicitly have [see Eqs. (A8a) and (A8b)]

$$f_{m_a}^{(n, m_a+m_b-n)}(\theta) = \frac{(-1)^{m_a+n}}{\sqrt{n!(m_a+m_b)_n}} \sqrt{\binom{m_a+m_b}{m_a}} [\cos(\theta/2)]^{m_b-n} [\sin(\theta/2)]^{m_a-n} g_{m_a}^{(n, m_a+m_b-n)}(\theta), \quad (6a)$$

$$g_{m_a}^{(n, m_a+m_b-n)}(\theta) = \delta_{m_a+m_b, n+m} \sum_{q=0}^n \binom{n}{q} (-1)^q (m_a)_{n-q} [\cos^2(\theta/2)]^{n-q} (m_b)_q [\sin^2(\theta/2)]^q \equiv g(m_a, m_b|n, m). \quad (6b)$$

Equations (6a) and (6b) are the primary equations of interest and their implications are the main focus of this work.

Let us now consider a general bipartite (in general, mixed) state ρ_{ab} impinging on the BS with input modes a and b . The probability $P(m_a, m_b, \theta)$ to measure m_a photons in the output mode a and m_b photons in the output mode b upon exit from the BS is given by

$$\rho_{ab} = \sum_{n, n', m, m'} \rho_{nm, n'm'} |n, m\rangle_{ab} {}_{ab} \langle n', m'| \xrightarrow{U(\theta)} \rho_{ab}^{(\text{out})} = \sum_{n, n', m, m'} \rho_{nm, n'm'} |n, m\rangle_{ab}^{(\text{out})} {}_{ab} \langle n', m'| \quad (7a)$$

$$\begin{aligned} \Rightarrow P(m_a, m_b, \theta) &= \text{Tr}[M_{ab} \rho_{ab}^{(\text{out})}] = \sum_{n, n', m, m'} \rho_{nm, n'm'} {}_{ab} \langle m_a, m_b | n, m \rangle_{ab}^{(\text{out})} {}_{ab} \langle n', m' | m_a, m_b \rangle_{ab} \\ &= \sum_{n, n', m, m'} \rho_{nm, n'm'} f_{m_a}^{(n, m_a+m_b-n)}(\theta) \delta_{m, m_a+m_b-n} f_{m_a}^{(n', m_a+m_b-n')}(\theta) \delta_{m', m_a+m_b-n'}. \end{aligned} \quad (7b)$$

Let us designate pure states in modes a and b as $|\psi\rangle_a = \sum_{n=0}^{\infty} c_n |n\rangle_a$ and $|\phi\rangle_b = \sum_{m=0}^{\infty} d_m |m\rangle_b$, respectively, with $\sum_{n=0}^{\infty} |c_n|^2 = \sum_{m=0}^{\infty} |d_m|^2 = 1$, and a mixed state ρ_b in mode b as $\sum_{m, m'=0}^{\infty} \rho_{m, m'}^{(b)} |m\rangle_b \langle m'|$ with $\sum_{m=0}^{\infty} \rho_{m, m}^{(b)} = 1$. Specializing the general case (7b) to interesting specific cases, we obtain

$$|\Psi_{\text{in}}\rangle_{ab} = |n, m\rangle_{ab} \Rightarrow P(m_a, m_b, \theta) = |f_{m_a}^{(n, m_a+m_b-n)}(\theta)|^2 \quad (\text{FS-FS case}), \quad (8a)$$

$$|\Psi_{\text{in}}\rangle_{ab} = |n, \phi\rangle_{ab} \Rightarrow P(m_a, m_b, \theta) = |d_{m_a+m_b-n}|^2 |f_{m_a}^{(n, m_a+m_b-n)}(\theta)|^2 \quad (\text{FS-PS case}), \quad (8b)$$

$$\rho_{ab}^{(\text{in})} = |n\rangle_a \langle n| \otimes \rho_b \Rightarrow P(m_a, m_b, \theta) = \rho_{m_a+m_b-n, m_a+m_b-n}^{(b)} |f_{m_a}^{(n, m_a+m_b-n)}(\theta)|^2 \quad (\text{FS-MS case}), \quad (8c)$$

$$|\Psi_{\text{in}}\rangle_{ab} = |\psi, \phi\rangle_{ab} \Rightarrow P(m_a, m_b, \theta) = \left| \sum_{n=0}^{\infty} c_n d_{m_a+m_b-n} f_{m_a}^{(n, m_a+m_b-n)}(\theta) \right|^2 \quad (\text{PS-PS case}), \quad (8d)$$

$$\begin{aligned}
|\Psi_{\text{in}}\rangle_{ab} &= |\psi\rangle_a \langle\psi| \otimes \rho_b \Rightarrow P(m_a, m_b, \theta) \\
&= \left| \sum_{n, n'=0}^{\infty} c_n c_{n'}^* \rho_{m_a+m_b-n, m_a+m_b-n'}^{(b)} f_{m_a}^{(n, m_a+m_b-n)}(\theta) f_{m_a}^{(n', m_a+m_b-n')}(\theta) \right|^2 \quad (\text{PS-MS case}), \quad (8e)
\end{aligned}$$

where we have used the denotations FS for Fock state, PS for pure state, and MS for mixed state and from now on drop the subscript ab on the output joint probability distribution $P(m_a, m_b, \theta)$.

The important point to note is that for Eqs. (8a)–(8c) with a single FS $|n\rangle_a$ in the a mode, we isolate a single beam-splitter coefficient (BSC) $f_{m_a}^{(n, m_a+m_b-n)}(\theta) \propto g(m_a, m_b, \theta)$ [Eq. (6b)]. Therefore, if $g(m_a, m_b, \theta) \rightarrow 0$, then the joint probability $P(m_a, m_b, \theta) \rightarrow 0$ independently of the amplitudes or density-matrix elements that define the b -mode input state. We will see shortly that this always occurs for the case of n odd (where n labels the FS of the a -mode input state) and for a 50:50 BS ($\theta = \pi/2$) when $m_a = m_b = m'$, i.e., $P(m', m', \pi/2) = 0$ for joint coincidences of the same number of photons in the output modes of the 50:50 BS. For the situations of a pure state in the a mode and either a pure or a mixed state in the b mode, from Eqs. (8d) and (8e) we see that we have additional sums over the amplitudes and/or density-matrix elements defining the a - and b -mode input states. However, if the a -mode state contains only a superposition of odd number of photons (FS), i.e., an odd-parity state, then when each of the BSCs is evaluated at $\theta = \pi/2$ for a 50:50 configuration each of the BSC will separately go to zero, independently of the amplitudes or density-matrix elements defining the states, and once again the diagonal of

$$\begin{aligned}
g(m_a, m_b, \theta|1) &= [m_a \cos^2(\theta/2) - m_b \sin^2(\theta/2)], \quad (9a) \\
g(m_a, m_b, \theta|2) &= [m_a \cos^2(\theta/2)(m_a - 1) \cos^2(\theta/2) - 2m_a \cos^2(\theta/2)m_b \sin^2(\theta/2) + m_b \sin^2(\theta/2)(m_b - 1) \sin^2(\theta/2)], \quad (9b) \\
g(m_a, m_b, \theta|3) &= [m_a \cos^2(\theta/2)(m_a - 1) \cos^2(\theta/2)(m_a - 2) \cos^2(\theta/2) - 3m_a \cos^2(\theta/2)(m_a - 1) \cos^2(\theta/2)m_b \sin^2(\theta/2) \\
&\quad + 3m_a \cos^2(\theta/2)m_b \sin^2(\theta/2)(m_b - 1) \sin^2(\theta/2) - m_b \sin^2(\theta/2)(m_b - 1) \sin^2(\theta/2)(m_b - 2) \sin^2(\theta/2)], \quad (9c)
\end{aligned}$$

where $P(m_a, m_b, \theta|n) \propto g^2(m_a, m_b, \theta|n)$. Here we have written $g(m_a, m_b, \theta|n)$ and $P(m_a, m_b, \theta|n)$ since the value of m is given by the δ function $\delta_{m_a+m_b, n+m}$ in Eq. (6b) that ensures that the total number of photons $m_a + m_b$ measured upon exit of the BS is equal to the total number of input photons n and m from the dual basis state $|n, m\rangle_{ab}$. We see that in Eq. (6b) and explicitly in Eqs. (9a)–(9c) that each factor of $(m_a - j)_{j \in \{0, \dots, [(n-k)-1]\}}$ in $(m_a)_{n-k}$ is associated with a factor of $T = \cos^2(\theta/2)$ and similarly that each factor of $(m_b - j)_{j \in \{0, \dots, (k-1)\}}$ in $(m_b)_k$ is associated with a factor of $R = \sin^2(\theta/2)$. Note that for a single a -mode input FS $|1\rangle_a$, Eq. (9a) indicates that individual nodes or zeros of $P(m_a, m_b, \theta|1)$ are given for a general BS angle θ by $\tan^2(\theta/2) = m_a/m_b$ and not just for the 50:50 BS case of BMG of $\theta = \pi/2 \Rightarrow m_a = m_b$. However, we are ultimately interested in nodal curves, i.e., curves of zeros representing complete destructive interference that occur for some relationship between m_a and m_b and for some angle θ . Our primary

the joint probability $P(m', m', \pi/2)$ will go to zero. The proof of these claims is developed in the next section.

III. ANGULAR PORTION $g(m_a, m_b, \theta)$ FOR A 50:50 BS

The focus of this section is to explore the angular portion $g(m_a, m_b, \theta)$ [Eq. (6b)] of the probability amplitude ${}_{ab}\langle m_a, m_b | n, m \rangle_{ab}^{(\text{out})}$ arising from the BS amplitude $f_p^{(n, m)}(\theta)$ [Eq. (4a)] of the transformed basis state $|n, m\rangle_{ab}^{(\text{out})} = U(\theta)|n, m\rangle_{ab}$ after the measurement M_{ab} is made of m_a and m_b photons in the output a and b modes, respectively. Of particular interest will be $g(m_a, m_b, \pi/2)$ in the 50:50 BS configuration $\theta = \pi/2$. It will be instructive to examine $g(m_a, m_b, \pi/2)$ explicitly in the case of low photon numbers $n \in \{1, 2, 3\}$ where it is easy to see how the symmetry in (m_a, m_b) gives rise to the interference effects that apply for general n . Later on, we return to these photon-number cases when we examine other than 50:50 BS angles.

A. $g(m_a, m_b, \theta)$: General case

In general, $g(m_a, m_b, \theta)$ is given by Eq. (6b), which generalizes Eqs. (7)–(10) of the angular portion of the formulas in Ref. [15]. For $n \in \{1, 2, 3\}$ Eq. (6b) explicitly yields

result is that we can always produce such a nodal line for a 50:50 BS ($\theta = \pi/2$) with $m_a = m_b = m'$ if the input state to mode a is an odd-numbered FS $|n = 2n' + 1\rangle_a$ regardless of the input state entering the b mode. Equation (6b) has a kind of hyperbinomial formula structure. The function $g(m_a, m_b, \theta|n)$ can be formally summed as

$$\begin{aligned}
g(m_a, m_b, \theta|n, m) &= \delta_{m_a+m_b, n+m} (m_a)_n [\cos^2(\theta/2)]^n {}_2F_1[-m_b, -n; 1 \\
&\quad + m_a - n; -\tan^2(\theta/2)], \quad (10)
\end{aligned}$$

where ${}_2F_1(a, b; c; z) = \sum_{k=0}^{\infty} \frac{(a)_k (b)_k}{(c)_k} \frac{z^k}{k!}$ is the hypergeometric function, with $x^{(n)} = (x+0)(x+1)(x+2) \cdots [x+(n-1)] = \frac{\Gamma(x+k)}{\Gamma(x)}$, and $x^{(0)} \equiv 1$, $x^{(1)} = x$, $x^{(2)} = x(x+1)$, etc., is the rising or ascending factorial function or Pochhammer symbol [27]. While Eq. (10) reproduces Eq. (6b), the former involves ratios of Γ functions of negative integers, which in-

dividually are infinite, but whose ratios are finite. Further, for a 50:50 BS ($\theta = \pi/2$) the function ${}_2F_1(-m_b, -n; 1 + m_a - n; -1)$ does not have a representation in terms of any simple known special function [28] whose properties we can exploit, while $g_{m_a}^{(n, m_a + m_b - n)}(\pi/2) \propto \sum_{q=0}^n \binom{n}{q} (-1)^q (m_a)_{n-q} (m_b)_q$ is precisely the functional (nearly binomial) form from which the interference effects discussed in this work can be easily inferred and derived. Therefore, we find Eq. (6b) more intuitively appealing and useful due to its hyperbinomial formula structure.

B. Effects at a 50:50 BS: CNL for n odd, $m_a = m_b = m$

An examination of Eq. (6b) reveals that it is invariant, up to a crucial overall sign $(-1)^n$, under the interchange of $m_a \leftrightarrow m_b$ and $\theta \rightarrow \pi - \theta$, i.e.,

$$g(m_b, m_a, \pi - \theta | n) = (-1)^n g(m_a, m_b, \theta | n). \quad (11)$$

This can be seen by noting that $\theta \rightarrow \pi - \theta$ exchanges $\cos(\theta/2) \leftrightarrow \sin(\theta/2)$. When setting $m_a \leftrightarrow m_b$ in Eq. (6b) we note that we can write the binomial coefficient $\binom{n}{q}$ as $\binom{n}{n-q}$. Defining $q' = n - q$ or $q = n - q'$ interchanges the indices q and $n - q$ to $n - q'$ and q' , respectively. Finally, the term $(-1)^q \rightarrow (-1)^{n-q'} = (-1)^n (-1)^{q'}$. Therefore, upon factoring out the term $(-1)^n$ we can relabel $q' \rightarrow q$ to finally arrive at Eq. (11).

Thus, for an input state $|n, m\rangle_{ab}$ and for the case of joint coincident counts with equal numbers of measured photons in each output port of a 50:50 BS, i.e., $\theta = \pi/2$ and $m_a = m_b \equiv m'$, Eq. (11) yields

$$|\Psi_{\text{in}}\rangle_{ab} = |n, m\rangle_{ab}, \quad 50:50 \text{ BS}(\theta = \pi/2), \\ m_a = m_b \equiv m'$$

$$g(m', m', \theta | n = 2n' + 1) = \frac{(m')_{n'}}{2^{3n'-1}} \cos(\theta) \text{poly}'_{n'}(m', \theta) \xrightarrow{\theta=\pi/2} 0 \quad \text{for } n = 2n' + 1 \text{ odd}, \quad (14a)$$

$$g(m', m', \theta | n = 2n') = \frac{(m')_{n'+1}}{2^{3n'-1}} \text{poly}'_{n'}(m', \theta) \neq 0 \quad \text{for } n = 2n' \text{ even}. \quad (14b)$$

In Eq. (14a) with $n' > 0$, $\text{poly}'_{n'}(m', \theta)$ is a polynomial of order n' in m and involves $\cos(k2\theta)$ terms for $k \in \{1, 2, \dots, n'\}$ such that $\text{poly}'_{n'}(m', \theta = \pi/2) \neq 0$. The crucial point is that for n odd, a factor of $\cos(\theta)$ can always be factored out of the full expression for $g(m', m', \theta | n)$ (see the formal proof in Appendix B), with $\cos(\theta = \pi/2) = 0$ for a 50:50 BS. For n even, no such trigonometric term factors out of the full expression for $g(m', m', \theta | n)$ in Eq. (14b). In Eq. (14b) $\text{poly}'_{n'}(m, \theta)$ has the same characteristics (form) as $\text{poly}'_{n'}(m, \theta)$ in Eq. (14a), most importantly that $\text{poly}'_{n'}(m, \theta = \pi/2) \neq 0$ for a 50:50 BS.

It should be noted that half the points on the CNL for the dual FS input $|n, m\rangle_{ab}^{(\text{in})}$ have $P(m', m', \pi/2 | n = \text{odd}) = 0$ trivially, since if m is even there simply is no output state $|m', m'\rangle_{ab}^{(\text{out})}$ with an equal number of photons for both the a and b modes. For example, for input state $|1, 2\rangle_{ab}^{(\text{in})}$, the output state $|1, 2\rangle_{ab}^{(\text{out})}$ from a 50:50 BS is spanned by the basis states $\{|0, 3\rangle_{ab}, |1, 2\rangle_{ab}, |2, 1\rangle_{ab}, |3, 0\rangle_{ab}\}$. Thus, no complete destructive interference is occurring (the HOM effect)

$$\Rightarrow g(m', m', \pi/2 | n) = (-1)^n g(m', m', \pi/2 | n) \xrightarrow{n \text{ odd}} 0 \\ \Rightarrow P(m', m', \pi/2 | n) \stackrel{n \text{ odd}}{=} 0. \quad (12)$$

That is, for n odd we have a CNL of contiguous zeros for all integers $m \in \mathbb{Z}_{\geq 0}$ in the b mode. This result depends solely on the intrinsic properties of the BS in a 50:50 configuration and is independent of the b -mode input FS state, as long as n is odd for the a -mode input Fock state.

The above result is evident in Eq. (9a), where for $\theta = \pi/2$ and $n = 1$ we have

$$g(m_a, m_b, \pi/2 | 1) = \frac{1}{4}(m_a - m_b) \xrightarrow{m_a=m_b} 0 \quad (13a)$$

and for $n = 3$ from Eq. (9c) we have

$$g(m_a, m_b, \pi/2 | 3) = \frac{1}{8} [(m_a)_3 - 3(m_a)_2(m_b)_1 \\ + 3(m_a)_1(m_b)_2 - (m_b)_3] \xrightarrow{m_a=m_b} 0. \quad (13b)$$

In general, for n odd there are $n + 1$ even number of terms in $g(m_a, m_b, \pi/2 | n)$ with a symmetric binomial coefficient $\binom{n}{q}$ with alternating signs $(-1)^q$ so that the first $(n + 1)/2$ terms have equal magnitude, but opposite signs of the latter $(n + 1)/2$ terms [e.g., for $n = 5$, the alternating binomial coefficients are $(1, -5, 10, -10, 5, -1)$]. When $m_a = m_b \rightarrow m$ as for a 50:50 BS, these even numbers of terms cancel in pairs to yield zero.

For $n = 1$, $g(m', m', \theta | n = 1) = m' \cos(\theta) \xrightarrow{\theta=\pi/2} 0$ for a 50:50 BS. A closer examination of Eqs. (6b) and (10) reveals the following behavior (obtained by induction) for $g(m', m', \theta | n)$ for n odd and even:

since a diagonal output state is simply not present. However, if m is also odd, then $n + m$ is even and the output contains the diagonal state $|m', m'\rangle_{ab}$ with $m' = (n + m)/2$ whose coefficient is proportional to $\cos(\theta) \xrightarrow{\theta=\pi/2} 0$. This is the HOM effect, i.e., complete destructive interference for the amplitude of the diagonal output state of a 50:50 BS. In a sense, the 50:50 BS acts like a (notch) filter that singles out FS output pairs $|m', m'\rangle_{ab}$ (with n and m both odd) and tags them with a factor proportional to $\cos(\theta)$, which can then be made zero for a 50:50 BS. For example, for input state $|1, 3\rangle_{ab}^{(\text{in})}$ the output states are spanned by $\{|0, 4\rangle_{ab}, |1, 3\rangle_{ab}, |2, 2\rangle_{ab}, |3, 1\rangle_{ab}, |4, 0\rangle_{ab}\}$ and the diagonal output state $|2, 2\rangle_{ab}$ has a coefficient proportional to $\cos(\theta)$ for a BS of arbitrary reflectivity. Note that the input state $|0, 4\rangle_{ab}^{(\text{in})}$ (as well as input states $|2, 2\rangle_{ab}^{(\text{in})}$ and $|4, 0\rangle_{ab}^{(\text{in})}$) also contains the diagonal output state $|2, 2\rangle_{ab}$. However, because n (and m) is even in this case one will not be able to factor out the term $\cos(\theta)$ from $f_{p=2}^{n=2, m=2}(\theta)$ and hence no HOM effect occurs.

Explicitly, for input states $|2, m\rangle$ there are no output states of the form $|m', m'\rangle_{ab}$ with m odd since that would imply that $m' = (n + m)/2$ would be a half-integer. For m even we have from Eq. (14b) that $P(m', m', \theta|n = 2) = \frac{1}{4}m'[2m' - 3 + (2m' - 1)\cos(2\theta)]$ for $m' = (n + m)/2$. Thus, input states $\{|2, 2\rangle_{ab}, |2, 4\rangle_{ab}, |2, 6\rangle_{ab}, \dots\}$ contain output states $\{|2, 2\rangle_{ab}, |3, 3\rangle_{ab}, |4, 4\rangle_{ab}, \dots\}$, respectively, but their coefficients are not proportional to $\cos(\theta)$. If we instead consider input states $|3, m\rangle_{ab}$, states with m even again simply do not produce diagonal output states. The remaining input states $\{|3, 1\rangle_{ab}, |3, 3\rangle_{ab}, |3, 5\rangle_{ab}, \dots\}$ with m odd do produce diagonal output states $\{|2, 2\rangle_{ab}, |3, 3\rangle_{ab}, |4, 4\rangle_{ab}, \dots\}$, respectively. From Eq. (14a) we have $P(m', m', \theta|n = 2) = \frac{1}{4}m'(m' - 1)\cos(\theta)[2m' - 7 + (2m' - 1)\cos(2\theta)]$, which is proportional to $\cos(\theta) \xrightarrow{\theta=\pi/2} 0$ and hence gives rise to the extended HOM effect for a 50:50 BS. [Note that for input states $|1, m\rangle_{ab}$, we have $P(m', m', \theta|n = 1) = m'\cos(\theta)$, with $m' = (1 + m)/2$, which again implies that the extended HOM effect occurs for $n = 1$ and m odd.]

The main result here is that for the dual FS input states $|n, m\rangle_{ab}$, with both n and m odd, the diagonal of the output joint probability distribution $P(m' = (n + m)/2, m', \theta|n) \propto \cos^2(\theta) \xrightarrow{\theta=\pi/2} 0$ for a 50:50 BS, which is an extended form of the HOM effect. These zeros make up half the points on the output diagonal CNL.

The above results apply to each two-mode FS basis input state $|n, m\rangle_{ab}$ entering the BS. However, since we can expand any b -mode pure state $|\psi\rangle_b = \sum_m d_m |m\rangle_b$ in terms of basis states $\{|m\rangle_b\}$, the above results also apply to any input state of the form $|n\rangle_a |\psi\rangle_b$. Therefore, Eq. (12) has wide-ranging universal implications. For a -mode input states that contain superpositions of only odd FSs, the probability $P(m_a, m_b, \theta)$ will involve the square of a sum of BSCs $g(m_a, m_b, \theta|n \rightarrow \text{odd})$, each of which goes to zero for a 50:50 BS and for $m_a = m_b$, regardless of the input state entering mode b , pure or mixed. This can be seen from the general formula for the joint photon probability

$$P(m_a, m_b, \theta) = \left(\frac{2}{\mathcal{N}}\right)^2 e^{-(|\alpha|^2 + |\beta|^2)} \left| \sum_{n=0}^{\infty} \frac{\alpha^n s_n}{\sqrt{n!}} \frac{\beta^{m_a+m_b-n}}{\sqrt{(m_a+m_b-n)!}} f_{m_a}^{(n, m_a+m_b-n)}(\theta) \right|_{m_a=m_b}^2 \xrightarrow{\theta=\pi/2} 0. \quad (15)$$

This occurs because the factor of s_n from the odd cat state ensures there are only odd values of n present and each BSC $f_{m_a}^{(n, m_a+m_b-n)} \propto g(m_a, m_b, \theta|n \rightarrow \text{odd}) \xrightarrow[m_a=m_b]{\theta=\pi/2} 0$, as discussed above. Note that the amplitudes of the input coherent state for $|\beta\rangle_b$ just go along for the ride here. Neither was it crucial what the amplitudes for the input state in mode a were. What was critical was the fact the one of the input states to the BS (here the a mode) had only an odd number of FSs, which then plucked out BSCs $f_p^{(n, m=m_a+m_b-n)}(\theta) \propto g(m_a, m_b, \theta|n)$ with odd n , each of which goes to zero for a 50:50 BS and for (number-resolved) coincident measurements with equal numbers of photons in each mode, i.e., $m_a = m_b$. That the CNL for a 50:50 BS with $m_a = m_b$ measurements is a general

distribution from Eqs. (8a)–(8e) when n (or n') is odd in each BSC $f_{m_a}^{(n, m_a+m_b-n)}(\theta)$. Such candidate example states include (but are not limited to) $(|1\rangle_a + |3\rangle_a)/\sqrt{2}$, a photon-added single-mode squeezed state (SMSS) $\cosh^{-1}(r)a^\dagger|\xi\rangle_a = S(\xi)|1\rangle_a$, with a SMSS $|\xi\rangle_a = S(\xi)|0\rangle_a = e^{(\xi a^2 - \xi^* a'^2)/2}|0\rangle_a = \frac{1}{\sqrt{\cosh(r)}} \sum_{n=0}^{\infty} e^{in\varphi} \tanh^n(r) \frac{\sqrt{(2n)!}}{n!2^n} |2n\rangle_a$, with $\xi = re^{i\varphi}$ [see [25], Eqs. (2.18) and (2.24)], which contains only odd-number FSs (see [25], Chap. 4.6, pp. 89–90), or equivalently a photon-subtracted single-mode squeezed state $e^{-i\varphi} \sinh^{-1}(r)a|\xi\rangle_a = S(\xi)|1\rangle_a$, and an odd cat state

$$|\alpha_c\rangle_a = \mathcal{N}^{-1}(|\alpha\rangle_a - |-\alpha\rangle_a) = 2\mathcal{N}^{-1} \left(e^{-|\alpha|^2/2} \sum_{n=0}^{\infty} \frac{s_n \alpha^n}{\sqrt{n!}} \right),$$

with

$$s_n \equiv \frac{1 - (-1)^n}{2} = \begin{cases} 0, & n \text{ even} \\ 1, & n \text{ odd} \end{cases}$$

and normalization factor $\mathcal{N} = (2 - 2e^{-2|\alpha|^2})^{1/2}$ [see [25], Chap. 4.1, Eqs. (4.2) and (4.4) with phase choice $\varphi = \pi$]. The joint photon-number probability $P(m_a, m_b)$ is plotted below for the above states in Fig. 4, clearly showing a CNL along the diagonal $m_a = m_b$.

The case of an odd cat state mixed with a CS is a simple illustrative example of how this CNL occurs for pure states of odd parity entering mode a and any pure state entering mode b [Eq. (8d)]. The odd cat state input can be written as $|\Psi_{\text{in}}\rangle_{ab} = |\alpha_c\rangle_a |\beta\rangle_b = 2\mathcal{N}^{-1} e^{-(|\alpha|^2 + |\beta|^2)/2} \sum_{n=0}^{\infty} \sum_{m=0}^{\infty} \frac{\alpha^n s_n}{\sqrt{n!}} \frac{\beta^m}{\sqrt{m!}} |n, m\rangle_{ab}$. As described previously, the BS transforms the input pair of dual basis FSs to $|n, m\rangle_{ab} \xrightarrow{U(\theta)} |n, m\rangle_{ab}^{(\text{out})} = \sum_{p=0}^n f_p^{(n, m)}(\theta) |p, n+m-p\rangle_{ab}$. Inserting this into the above and projecting onto $|m_a, m_b\rangle_{ab}$ for the measurement of m_a photons in mode a and m_b photons in mode b (which produces the δ functions δ_{p, m_a} and δ_{m, m_a+m_b-n}) and performing the sum over p and m , we obtain

universal result is illustrated in Fig. 4 for the representative case of a CS of amplitude $\beta = 3$ ($\bar{n}_b = |\beta|^2$) in mode b mixed with various a -mode states containing only odd numbers of photons, including $|3\rangle_a$ [Fig. 4(a)] (the black solid diagonal line is the CNL), $(|1\rangle_a + |3\rangle_a)/\sqrt{2}$ [Fig. 4(b)], the photon-added single-mode squeezed state $a^\dagger|\text{SMSS}\rangle_a$ [Fig. 4(c)], and the odd cat state $|\alpha_c\rangle_a$ [Fig. 4(d)].

The main results of this section can be summarized as follows: For the measurement of the joint probability distribution $P(m', m', \pi/2|n)$ with equal numbers of photons in both output modes of a 50:50 BS we have, for $n = 2n' + 1$ odd, $P(m', m', \pi/2|2n' + 1) \propto g^2(m, m, \pi/2|2n' + 1) \equiv 0$, regardless of the input state in mode b , pure or mixed, which we term a (diagonal) central nodal line [see Eq. (14a)], and

for $n = 2n'$ even, $P(m', m', \pi/2|2n') \propto g^2(m, m, \pi/2|2n') \neq 0$ [see Eq. (14b)].

IV. PSEUDONODAL CURVES FOR A 50:50 BS AND A NON-50:50 BS

As we have seen in the preceding section, central nodal lines exist for a -mode input states containing superpositions of odd-numbered FSs (or individual n -odd FSs) when detecting $m_a = m_b$ for a 50:50 BS with $\theta = \pi/2$. These are the CNLs in the bottom rows of Fig. 2 for $P(m_a, m_b|n = 1)$ and Fig. 3 for $P(m_a, m_b|n = 3)$ for a FS $|n\rangle_a$ mixed with a CS $|\beta\rangle_b$ (left column) and TS ρ_b (right column).

In addition to the CNLs, we also observe in Figs. 2–4 what appear to be PNCs [e.g., the black dashed lines in Fig. 4(a) passing through the blue dots, which have value zero] symmetrically placed about the center line (diagonal) $m_a = m_b$ [e.g., black solid line in Fig. 4(a)] of the joint output photon-number distribution for all $n > 0$, even or odd, when in a 50:50 BS configuration. We now seek to understand and quantify their origin. Without a loss of generality, we will explore the case of an initial FS-CS input $|\Psi_{\text{in}}\rangle_{ab} = |n\rangle_a|\beta\rangle_b$ for $n = 2, 3$ in Figs. 3(a) and 3(c), respectively, and for $n = 3$ in Fig. 4(a) and recall that $P(m_a, m_b, \theta) \propto [g(m_a, m_b, \theta)]^2$.

For a dual FS basis input state $|n, m\rangle_{ab}$ the expressions for $g(m_a, m_b, \theta|n)$ for $n = 2, 3$ are given by

$$g(m_a, m_b, \theta|2) = m_a(m_a - 1)[\cos^2(\theta/2)]^2 - 2m_a m_b [\cos^2(\theta/2)][\sin^2(\theta/2)] + m_b(m_b - 1)[\sin^2(\theta/2)]^2 \quad (16a)$$

$$\xrightarrow{\theta \rightarrow \pi/2} \frac{1}{4}[m_a(m_a - 1) - 2m_a m_b + m_b(m_b - 1)] \quad (16b)$$

$$\xrightarrow{\theta \rightarrow \pi/3} \frac{1}{16}[9m_a(m_a - 1) - 3m_a m_b + m_b(m_b - 1)], \quad (16c)$$

$$g(m_a, m_b, \theta|3) = m_a(m_a - 1)(m_a - 2)[\cos^2(\theta/2)]^3 - 3m_a(m_a - 1)m_b[\cos^2(\theta/2)]^2[\sin^2(\theta/2)] + 3m_a m_b(m_b - 1)[\cos^2(\theta/2)][\sin^2(\theta/2)]^2 + m_b(m_b - 1)(m_b - 2)[\sin^2(\theta/2)]^3 \quad (16d)$$

$$\xrightarrow{\theta \rightarrow \pi/2} \frac{1}{8}[m_a(m_a - 1)(m_a - 2) - 3m_a(m_a - 1)m_b + 3m_a m_b(m_b - 1) - m_b(m_b - 1)(m_b - 2)] \quad (16e)$$

$$\xrightarrow{\theta \rightarrow \pi/3} \frac{1}{64}[27m_a(m_a - 1)(m_a - 2) - 27m_a(m_a - 1)m_b + 9m_a m_b(m_b - 1) - m_b(m_b - 1)(m_b - 2)], \quad (16f)$$

where we have evaluated the expressions for the two angles $\theta = \pi/2$ (50:50 BS) and $\theta = \pi/3$ (non-50:50 BS).

A. PNCs for a 50:50 BS

A necessary condition for the existence of solutions of $g(m_a, m_b, \theta|n) = 0$ for integer values of (m_a, m_b) is that the above polynomials in m_a and m_b have integer coefficients, which occur when $T = \cos^2(\theta/2)$, and hence $R = \sin^2(\theta/2)$, is a rational number, i.e., a fraction given by the ratio of integers. For the cases chosen $\theta = \pi/2$ (50:50 BS) yields $(\cos^2(\theta/2), \sin^2(\theta/2)) = (1/2, 1/2)$, and for $\theta = \pi/3$ (non-50:50 BS) $(\cos^2(\theta/2), \sin^2(\theta/2)) = (3/4, 1/4)$. Polynomial equations with integer coefficients and integer solutions are known as Diophantine polynomials. Isolated zeros of these equations can be found by a simple brute force search (BFS) over integer values of (m_a, m_b) . Analytic solutions can be found by various different methods, one of which is by assuming a parametric form of $(m_a(k), m_b(k))$ in terms of another integer $k \in \mathbb{Z}$. For a 50:50 BS ($\theta = \pi/2$) and low values of n , we have found that quadratic polynomials in k of the parametric form $m_a(k) = a_0 + a_1 k + a_2 k^2$ and $m_b(k) = b_0 + b_1 k + b_2 k^2$, with $\{a_0, a_1, a_2, b_0, b_1, b_2\} \in \mathbb{Z}$ again integers, are sufficient to find analytic solutions for the PNCs in the cases of $n = 2$ and 3 for a 50:50 BS, i.e., $P(m_a(k), m_b(k), \pi/2|n) = 2, 3) \equiv 0$, identically.

In Fig. 5 we plot the case of a 50:50 BS ($\theta = \pi/2$) for $g(m_a, m_b, \theta = \pi/2|n = 2)$ [Fig. 5(a)] and $g(m_a, m_b, \theta = \pi/2|n = 3)$ [Fig. 5(b)] with the plot markers indicating the zeros arising from polynomials $(m_a(k), m_b(k))$ (for

$m_a \neq m_b$), which lie on the solid curves (the PNCs). An example of such a parametric solutions for $n = 2$ is $(m_a(k), m_b(k)) = (2k^2 - k, 2k^2 - 3k + 1)$, while for

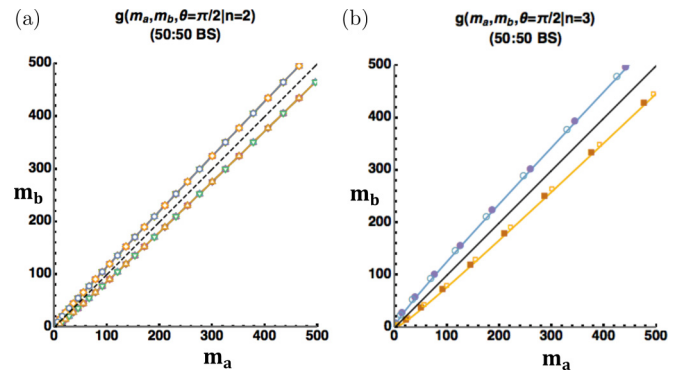


FIG. 5. Plots of zeros of (a) $g(m_a, m_b, \theta = \pi/2|n = 2)$ and (b) $g(m_a, m_b, \theta = \pi/2|n = 3)$ for a 50:50 BS with $\theta = \pi/2$. Closed plot markers show upper and lower branch solutions analytically found by Reduce [29] in *Mathematica* and open markers show upper and lower branch solutions found by a BFS over approximately 11.4×10^6 (left) and 9.5×10^8 (right) 6-tuple integer coefficients $(a_0, a_1, a_2, b_0, b_1, b_2)$ of two quadratic polynomials (in k , an integer) for $(m_a = a_0 + a_1 k + a_2 k^2, m_b = b_0 + b_1 k + b_2 k^2)$, which identically solve $g(m_a, m_b, \theta = \pi/2|n) = 0$ analytically (see Tables II and III in Appendix C). Note that the black dashed line in (a) is the diagonal drawn for symmetry for $n = 2$, while the solid black line in (b) is the CNL for $n = 3$.

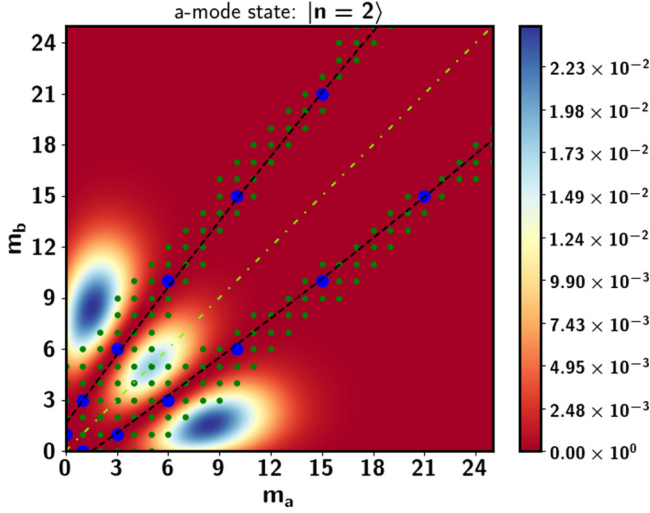


FIG. 6. Contour plot of the output joint probability $P(m_a, m_b, \theta = \pi/2)$ in Fig. 3(a) for input state $|2\rangle_a|\beta\rangle_b$ with PNCs (nondiagonal black dashed curves). The blue circles are points for which $g(m_a, m_b, \pi/2|n=3) \equiv 0$ through which the PNCs pass. The green dots are points for which $dg(m_a, m_b, \pi/2|n=3)/dm_a = 0$ (extremal values of near, but not complete, destructive interference). The yellow dot-dashed line is drawn to highlight the diagonal symmetry.

$n = 3$ an example is $(m_a(k), m_b(k)) = (6k^2 + 7k + 2, 6k^2 + 13k + 7)$ (see Tables II and III, respectively, in Appendix C). The black dashed central (symmetry) line represents a CNL solution ($m_a = m_b$) only for $n = 3$. For $n = 2$ we have drawn it as a diagonal in order to see the symmetric behavior of the plotted points. In both cases $n = 2, 3$, the colored solid lines in Fig. 5 are the PNCs on which the (isolated, noncontiguous) zeros (indicated by the plot markers) of $g(m_a, m_b, \theta = \pi/2|n = 2, 3)$ lie that were generated from the quadratic polynomial solutions $(m_a(k), m_b(k))$.

For the case of $n = 3$ we have overlaid the CNL [black solid diagonal line of complete destructive interference $g(m', m', \pi/2|n = 3) = 0$] and the PNC (black dashed non-diagonal curve) of Fig. 5(a) onto the contour plot of Fig. 4(a). The blue dots in the latter plot are the points $(m_a, m_b \neq m_a)$ of complete destructive interference where $g(m_a, m_b, \pi/2|n = 3) = 0$ through which the PNCs (black dashed curves) pass. Along the PNC, in between the zero values (blue dots), $g(m_a, m_b, \pi/2|n = 3)$ obtains nearly (but not) complete destructive interference (fringes), i.e., extremal values. This statement is most clearly illustrated by explicitly examining the case of $n = 2$ for the input state $|2\rangle_a|\beta\rangle_b$ in Fig. 3(a) as well as in Fig. 6.

For $n = 2$ we have $g(m_a, m_b, \pi/2|n = 2) = 1/4[m_a(m_a - 1) - 2m_a m_b + m_b(m_b - 1)]$ [Eq. (16b)]. Temporarily treating m_a and $m_b \equiv m_b(m_a)$ as continuous variables, let us formally solve $dg(m_a, m_b, \pi/2|n = 2)/dm_a = 0$ for $\frac{dm_b}{dm_a} = \frac{2(m_b - m_a) + 1}{2(m_b - m_a) - 1}$. Solving this ordinary differential equation for $m_b(m_a)$ yields $m_b^{(\pm)} = m_a + \frac{1 \pm \sqrt{1 + 8m_a + k}}{2}$, where $k \in \mathbb{Z}$ is an arbitrary integration constant such that for $m_a \in \mathbb{Z}_{\geq 0}$ we accept only integer solutions of $m_b \in \mathbb{Z}_{\geq 0}$. [An obvious example solution is $(m_a = 1, k = 0)$ leading to solutions

$(m_a = 1, m_b^{(+)} = 3)$ and $(m_a = 1, m_b^{(-)} = 0)$.] These are the green dots in Fig. 6 [$(m_a, m_b^{(+)})$ and $(m_a, m_b^{(-)})$ upper and lower branches, respectively], the center of which is where the PNCs lie, as well as the exact zeros (blue dots) of $g(m_a, m_b, \pi/2|n = 2)$. While $dg(m_a, m_b, \pi/2|n = 2)/dm_a$ is not a proper derivative (since m_a and m_b are discrete), the points along which it takes zero values (green dots) are extremal points of near, but not complete, destructive interference (fringes), i.e., valleys of the output joint probability distribution. The valley floor is the PNCs (black dashed lines) of minimal values, along which are scattered exact zeros (blue dots) of $g(m_a, m_b, \pi/2|n = 2)$ representing nondiagonal points of complete destructive interference. Thus, we can say for PNCs of general n that $\{(m_a, m_b)|g(m_a, m_b, \pi/2|n) = 0\} \subset \{(m_a, m_b)|dg(m_a, m_b, \pi/2|n)/dm_a = 0\}$ (i.e., blue dots \subset green dots). These PNCs furcate (multiply divide) the output joint probability distribution into peaks and carved out valleys, as evident in Figs. 2 and 3.

B. PNCs for a non-50:50 BS

The question naturally arises whether such polynomial solutions $(m_a(k), m_b(k))$ also exist for non-50:50 BS angles $\theta \neq \pi/2$ again with $(T = \cos^2(\theta/2), R = \sin^2(\theta/2))$ rational numbers. The primary difference in the form of the Diophantine equations for arbitrary BS angles is now the integer coefficients are not alternating symmetric [i.e., of the binomial form $\binom{n}{q}(-1)^q$] as in the 50:50 BS case. In Fig. 7(a) we plot the PNCs for $g(m_a, m_b, \theta = \pi/3|n = 2)$ for a non-50:50 BS angle $\theta = \pi/3$, again with the colored solid lines indicating the PNCs on which the (isolated, noncontiguous) zeros (indicated by the plot markers) of $g(m_a, m_b, \theta = \pi/3|n = 2)$ lie which are generated from the quadratic polynomial solutions $(m_a(k), m_b(k))$. An example of such a parametric solution for $n = 2$ is $(m_a(k), m_b(k)) = (12k^2 + k, 36k^2 - 9k)$ (see Table IV in Appendix C). The (non-CNL) black dashed line $m_a = m_b$ is drawn to simply draw attention to the rotation of the PNC from this diagonal symmetry line from the previous 50:50 BS solution. Figure 7(a) is a contour plot blowup of the lower (m_a, m_b) pair region.

Finding analytic solutions for $g(m_a, m_b, \theta = \pi/3|n = 3)$ for the same non-50:50 BS angle of $\theta = \pi/3$ (Fig. 8) has proven to be problematic. Isolated zeros are easily found by a BFS double looping over $m_a, m_b \in \{1, \dots, 10^4\}$ producing $(m_a, m_b) \in \{(1, 0), (1, 1), (1, 11), (2, 0), (3, 1), (11, 55), (70, 162)\}$. The candidate solutions $(m_a, m_b) \in \{(1, 0), (1, 1), (2, 0)\}$ are trivially nonphysical due to the δ -function constraint $\delta_{m_a+m_b, n+m}$ since $n + m \geq 3$ for the FS input state $|3\rangle_a$. A BFS over quadratic polynomials of the form $m_a(k) = a_0 + a_1k + a_2k^2$ and $m_b(k) = b_0 + b_1k + b_2k^2$ with $\{a_0, a_1, a_2, b_0, b_1, b_2\} \in \mathbb{Z}$ with both coefficients a_k and b_k in the search range $\{-10, 50\}$ (i.e., 51.5×10^9 6-tuples) failed to produce any analytic solutions. Similarly, another BFS over cubic polynomials of the form $m_a(k) = a_0 + a_1k + a_2k^2 + a_3k^3$ and $m_b(k) = b_0 + b_1k + b_2k^2 + b_3k^3$ with $\{a_0, a_1, a_2, a_3, b_0, b_1, b_2, b_3\} \in \mathbb{Z}$ with both coefficients a_k and b_k in the search range $\{-10, 10\}$ (i.e., 37.8×10^9 8-tuples) also failed to produce any analytic solutions. These numerical searches for exact polynomial solutions

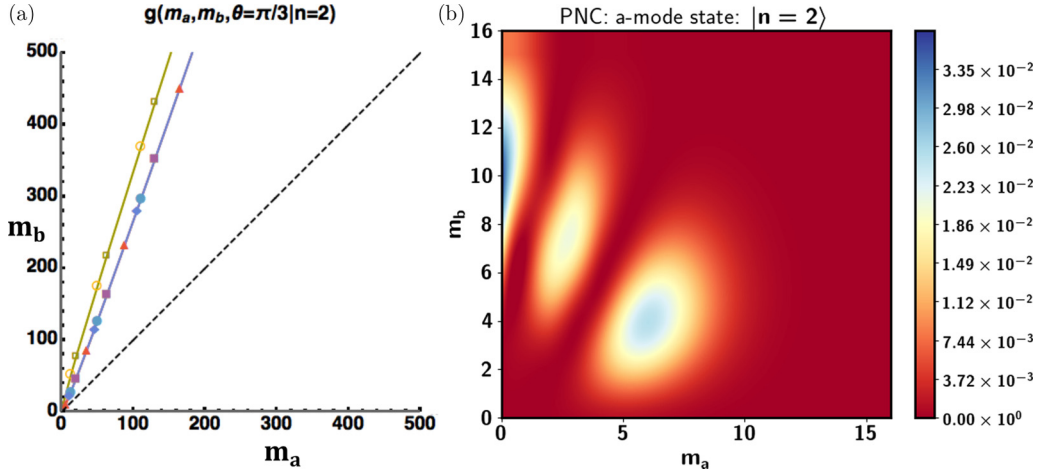


FIG. 7. (a) Plots of zeros of $g(m_a, m_b, \theta = \pi/3 | n=2)$ for a non-50:50 BS with $\theta = \pi/3$. Closed plot markers show upper branch solutions analytically found by Reduce in *Mathematica* and open markers show the lower branch solutions found by BFS over approximately 9.6×10^8 6-tuple integer coefficients ($a_0, a_1, a_2, b_0, b_1, b_2$) of two quadratic polynomials (in k , an integer) for ($m_a = a_0 + a_1k + a_2k^2, m_b = b_0 + b_1k + b_2k^2$) which identically solve $g(m_a, m_b, \theta = \pi/3 | n=2) = 0$ analytically. See Table IV of Appendix C. (b) Contour plot blowup of the lower (m_a, m_b) pair region for a coherent b -mode input state.

$(m_a(k), m_b(k))$ of parametric form in $k \in \mathbb{Z}$ clearly do not exclude the possibility for other forms of analytic solutions [e.g., solutions of cubic equations, if one naively solves $g(m_a, m_b, \pi/3 | n=3) = 0$ for $m_b(m_a)$ as a function of m_a , requiring $m_b \in \mathbb{Z}_{\geq 0}$ [29]].

As a conjectured explanation for the failure to find many zeros for $g(m_a, m_b, \pi/3 | n=3)$ it should be noted that as we rotate the BS angle from $\theta = \pi/2$ (50:50) to either extreme $\theta = 0$ ($T = 1$) or $\theta = \pi$ ($R = 1$) the polynomial $g(m_a, m_b, \theta | n)$ for general θ and n degenerates to either $(m_a)_n$ or $\pm(m_b)_n$ respectively, since $(\cos^2(\theta/2), \sin^2(\theta/2)) \rightarrow \{(1, 0), (0, 1)\}$, respectively, where no PNCs exist. That is, as we rotate θ any PNCs that lie symmetrically placed about the CNL (n odd) or diagonal $m_a = m_b$ (n even) must eventually vanish. We conjecture that this vanishing of the PNC for non-50:50 BS angles happens more severely in $g(m_a, m_b, \theta | n)$ for $n \geq 3$.

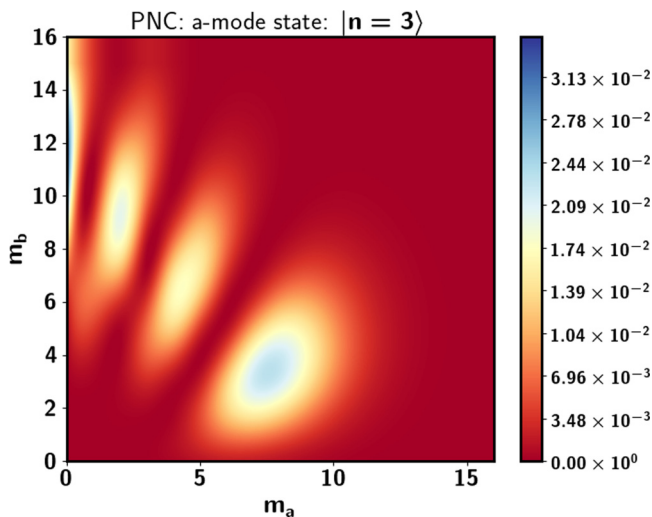


FIG. 8. Same as Fig. 7(b), except for $n = 3$, with $g(m_a, m_b, \theta = \pi/3 | n=3)$.

V. PROSPECTS FOR EXPERIMENTAL REALIZATION

The potential for experimental realization of the CNLs and PNCs discussed in this work rests on the ability to perform photon-number-resolving detection. Most detectors such as avalanche photodiode detectors are “bucket” detectors, meaning that they record either no signal (in the absence of spurious dark counts, which are always present, but quantifiable) or a single “click” from the collection of photons that enter the detector in the sampling window. Such click–no-click detectors can be multiplexed to achieve a quasi-photon-number resolution [23]. However, in those cases the fidelity of the measured state is always degraded compared to true or intrinsic photon-number-resolving detection. In many applications, however, multiplexed click detectors are sufficient to achieve high-fidelity state characterization [23].

Since 1998, great progress has been made in the development of true number-resolving detectors, specifically superconducting transition edge sensors (TESs). In contrast to simple click–no-click detectors, the TES output contains information about the number of photons absorbed. Transition edge sensors are highly sensitive microcalorimeters that are used as microbolometers to detect radiation from submillimeter wavelengths to γ rays. From the review article by Gerrits *et al.* [23], the optical TES is a superconducting sensor measuring the amount of heat absorbed from an optical photon with energy on the order of 1 eV. When an optical photon is absorbed by the sensor, the associated photon energy is transformed into a measurable temperature change of the sensor. Typical TESs operate at temperatures below 1 K. Transition edge sensors typically resolve photons over a range from 1 to 10 or 20, depending on the wavelength, heat capacity of the device, and steepness of the superconducting resistance transition.

Germane to our consideration, Gerrits *et al.* [23] have measured a coherent state with mean photon number $|\beta|^2 \approx 5$ using an optimum filter analysis to determine the pulse-height histogram. Well-defined nonoverlapping peaks for zero to four

photons are clearly discernible [see Fig. 2.8(c) of [23]]. Recently, Schmidt *et al.* [24], using quantum-dot-based photon sources emitting at 932 nm (1.33 eV), have reported that adjacent photon-number states up to 25 photons can be discriminated with the TES detectors with efficiencies exceeding 87% using principal component (PC) analysis (see Fig. 3 of [24]). In the optical regime an exemplary analog signal output of zero to six photons can be clearly distinguished by pulse heights at a wavelength of 653 nm (1.9 eV) (see Fig. 1, bottom and middle, of [24]). In these experiments each photon state in the photon-number distributions obtained from the pulse area and the PC analyses is fitted with a Gaussian function. The corresponding full width at half maximum is interpreted as the energy resolution ΔE_{FWHM} of the TES detectors.

Thus, the prospect to observe the predicted CNLs and PNCs by plotting as a histogram the photon-number-resolved output of the BS in the range $(m_a, m_b) \in \{0, 1, 2, 3, 4, 5\}$ seems very promising. This of course assumes that one can prepare a -mode input states with only odd numbers of photons (odd-parity state), such as odd-numbered FSs, photon-added or photon-subtracted single-mode squeezed states, or, e.g., an odd (coherent-state-based) cat state. The most promising of these prospects that appears most readily achievable with today's current technology is an input state consisting of a single-photon FS $|1\rangle_a$ in the a mode (obtained by heralding on either the signal or idler component of a biphoton two-mode squeezed state), mixed with either a weak CS or possibly a weak TS [see Figs. 2(c) and 2(d)] with a midrange mean photon number around $\bar{n} \approx 3$.

Realistic experiments will always involve the use of imperfect detectors. The inclusion of loss is easily performed by averaging the joint photon-number distribution $P(m_a, m_b, \theta)$ over a Bernoulli distribution with a Beer's law loss parameter (detector efficiency, probability) given by $0 \leq \eta = e^{-2\gamma L} \leq 1$, as discussed by LBK [21] and more recently by Laiho *et al.* [22]. The basic idea is that if m_a photons are detected in the a -mode output of the BS, it could have resulted from a total of $M_a \geq m_a$ photons, all of which (except for m_a) were lost, and hence not registered by the detector. The same is true for the detection of m_b photons in the b -mode output of the BS.

Let us define the a -mode projection operator

$$\Pi_a = \sum_{M_a \geq m_a} \binom{M_a}{m_a} \eta^{m_a} (1 - \eta)^{(M_a - m_a)} |M_a\rangle \langle M_a| \quad (17)$$

and an analogous expression for Π_b . The Bernoulli factor in the summation is the probability for m_a a -mode photons to traverse the BS with detection probability η per photon, with the remaining $M_a - m_a$ suffering loss (nondetection) with probability $1 - \eta$. These latter $M_a - m_a$ "lost" photons can be considered as having been "reflected" into a scattering mode with probability $R = 1 - \eta$, which is then not observed [e.g., via an additional virtual BS with transmissivity $T = \eta$ and $R = 1 - \eta$ (see Ref. [30] and Appendix C of [31])]. Note that as the detector efficiency goes to unity $\eta \rightarrow 1$, implying no loss, the factor $(1 - \eta)^{(M_a - m_a)}$ is nonzero only when $M_a = m_a$ and the projection operator collapses to $\Pi_a \xrightarrow{\eta \rightarrow 1} |m_a\rangle_a \langle m_a|$.

The output joint probability distribution $\tilde{P}(m_a, m_b, \theta; \eta_a, \eta_b)$ of the BS, with efficiencies η_a and

η_b in modes a and b , respectively, is now given by

$$\begin{aligned} \tilde{P}(m_a, m_b, \theta; \eta_a, \eta_b) &= \text{Tr}_{ab} [\Pi_a \otimes \Pi_b \rho_{ab}^{(\text{out})}] \\ &= \sum_{M_a \geq m_a} \sum_{M_b \geq m_b} \eta_a^{m_a} (1 - \eta_a)^{(M_a - m_a)} \\ &\quad \times \eta_b^{m_b} (1 - \eta_b)^{(M_b - m_b)} P(M_a, M_b, \theta). \end{aligned} \quad (18)$$

In Fig. 9 we plot the output joint probability distribution $P(m_a, m_b, \pi/2 | n = 1)$ for a FS-CS input $|\Psi_{\text{in}}\rangle_{ab} = |1\rangle_a |\beta\rangle_b$ for an ideal lossless 50:50 BS with mean number of photons $\bar{n}_b = |\beta|^2$ in the b mode. Figure 9(a) is for $\bar{n}_b = 1$, while Fig. 9(b) is for $\bar{n}_b = 3$. The probability distribution matrix is plotted directly below in the second row for the corresponding plot immediately above, with rows m_a and columns m_b labeled by the indices $(m_a, m_b) \in \{0, 1, 2, 3, 4, 5\}$. Due to the small average photon numbers used in the a - and b -mode input states, dictated by the discriminating capability of current (e.g., TES) photon-number-resolving detectors, by the time we get to $m_a, m_b = 3$ we must be able to distinguish a nonzero probability for joint photon detection from zero probability to roughly 1%. While challenging, such measurements are nonetheless within the realm of possibility with today's current technology.

In Fig. 10 we show the same plot as in Fig. 9 but now with the inclusion of loss, with $\eta_a = \eta_b = \eta = 0.95$ (5% loss) in Eq. (18). The diagonal CNL is no longer exactly zero due to the presence of a small amount of loss, but there is still a discernible nearly central nodal line that furcates the output joint probability distribution. It should be noted that losses in a quantum integrated waveguide-coupler BS can be as low as 1%.

To see the effect of loss on the nondiagonal PNC, we plot in Fig. 11 the output joint probability distribution $P(m_a, m_b, \pi/2 | n)$ for $n = 2$ [Figs. 11(a) and 11(c)] and $n = 3$ [Figs. 11(b) and 11(d)] with inclusion of loss $\eta_a = \eta_b = \eta = \{1.0, 0.95\} \leftrightarrow \{0\%, 5\%\}$ [Figs. 11(a) and 11(b) and Figs. 11(c) and 11(d), respectively] for a FS-CS input $|\Psi_{\text{in}}\rangle_{ab} = |n = 2, 3\rangle_a |\beta = \sqrt{3}\rangle_b$ for a 50:50 BS with mean number of photons in the b mode $\bar{n}_b = |\beta|^2 = 3$. While the degradation of the CNL for $n = 3$ is clearly discernible [Figs. 11(b) and 11(d)] with the inclusion of a small amount of loss, one can also observe the increase in the "valley floor" for the PNC, for both $n = 2$ and $n = 3$, illustrated in Figs. 11(c) and 11(d) with 5% loss ($\eta = 0.95$), over that of the ideal BS (no loss $\eta = 1.0$) in Figs. 11(a) and 11(b). These results indicate that experimental observation of the CNL and PNC in the presence of a small amount of noise is within the realm of possibility, modulo the difficulty or complexity of creating an a -mode input FS (especially for $n > 1$).

The difficulty in observing the PNC for the $|2\rangle_a |\beta\rangle_b$ FS-CS input in Figs. 11(a) and 11(c) is of course the preparation of the $n = 2$ a -mode FS. One possibility is to first use another canonical HOM setup with a single photon in each of the input ports (a' and b') of a 50:50 BS [generated from two multiplexed spontaneous parametric down-conversion (SPDC) sources, each of which heralds on its own idler], in order to create two separate signal photons $|1, 1\rangle_{a'b'}$. When these two

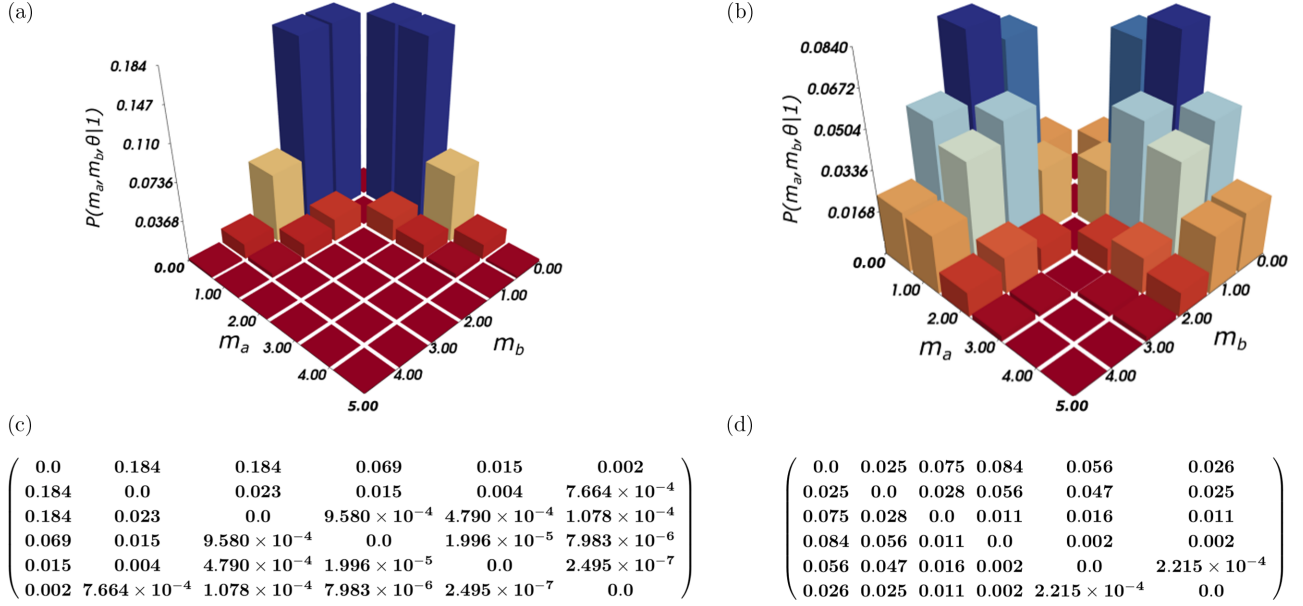


FIG. 9. Output joint probability distribution $P(m_a, m_b, \pi/2 | n = 1)$ for a FS-CS input $|\Psi_{in}\rangle_{ab} = |1\rangle_a |\beta\rangle_b$ for a 50:50 BS with the mean number of photons in the b mode $\bar{n}_b = |\beta|^2$: (a) $\bar{n}_b = 1$ and (b) $\bar{n}_b = 3$. (c) and (d) Probability matrix $P(m_a, m_b, \pi/2 | n = 1)$ for the plot in (a) and (b), respectively, with rows m_a and columns m_b labeled by the indices $(m_a, m_b) \in \{0, 1, 2, 3, 4, 5\}$.

photons enter a 50:50 BS, the output amplitude for the state $|1, 1\rangle_{a'b'}$ will suffer complete destructive interference, leading to the output state $|1, 1\rangle_{a'b'}^{(out)} = (|2, 0\rangle_{a'b'} + |0, 2\rangle_{a'b'})/\sqrt{2}$ from Eq. (2). If one then heralds on a null measurement [7,32] in the a' -mode output, then two photons must emerge in the b' -mode output (and vice versa), which can subsequently be used as the a -mode $n = 2$ FS input state $|2\rangle_a |\beta\rangle_b$ for Figs. 11(a) and 11(c). This null measurement occurs with probability 1/2, if the time delay between the two a' and b' input photons arriving at the first BS is zero.

The advantage of the above measurement scheme is that it does not require the use of number-resolving photon detection. However, if one does have access to number-resolving photon detection (e.g., a TES discussed above), then a straightforward scheme to generate a two- or three-photon FS is to simply herald one arm of a (biphoton) two-

mode squeezed state (TMSS) $|\xi\rangle_{a'b'} = \sum_{n=0}^{\infty} \sqrt{p_n^{(\xi)}} |n, n\rangle_{a'b'}$, where $p_n^{(\xi)} = \tanh^{2n}(r)/\cosh^2(r)$ with squeezing parameter $r > 0$. The amount of squeezing (in decibels) is given by $10 \log_{10}[(\Delta X)^2/(1/4)] = 10 \log_{10}[e^{-2r}]$ [25,26,33], where $(\Delta X)^2$ is the variance of the quadrature that undergoes squeezing and 1/4 (in these units) is the variance of the vacuum state. Typical values of r for strongly squeezed sources are in the range of $r \approx 1.4$ – 1.6 , leading to -12.2 to -13.9 dB of squeezing (for comparison, -3 dB of squeezing corresponds to $r = 0.35$).

We are now interested in the probability to detect the a' -mode FS state $|n\rangle_{a'}$ from the TMSS source $|\xi\rangle_{a'b'}$ with a number-resolving photon detector with efficiency (detection probability) η . Following Motes *et al.* [34] and Nunn *et al.* [32], the conditional probability $P_D(t|n')$ to detect t photons given that $n' \geq t$ were actually present is given

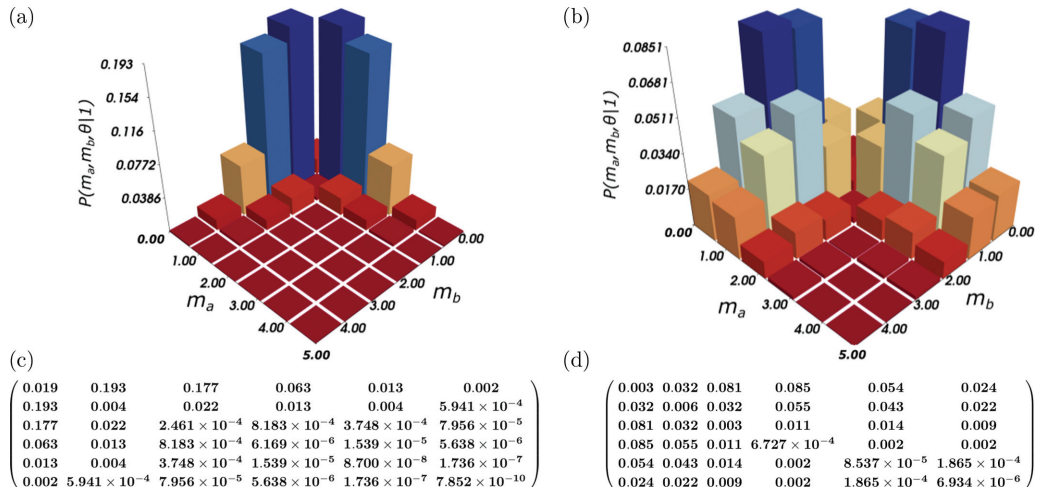


FIG. 10. Same as Fig. 9 but with the inclusion of loss: $\eta_a = \eta_b = \eta = 0.95$ (5% loss) in Eq. (18).

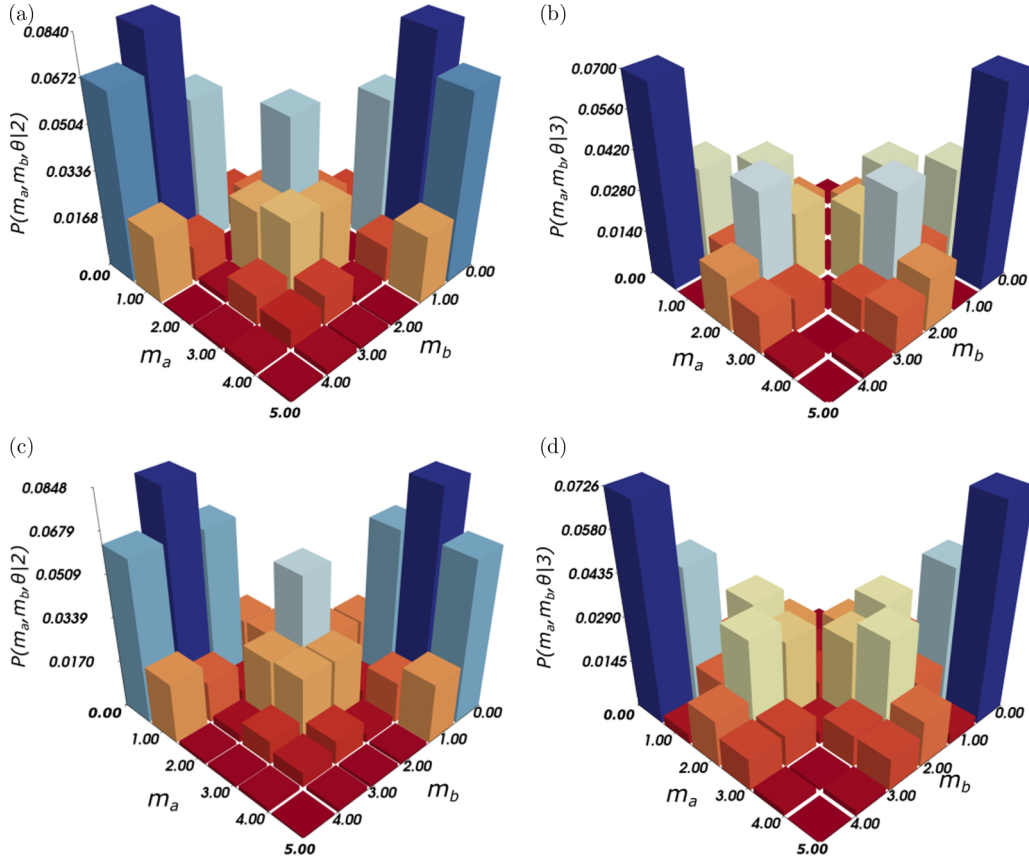


FIG. 11. Output joint probability distribution $P(m_a, m_b, \pi/2|n)$ for (a) and (c) $n = 2$ and (b) and (d) $n = 3$, with inclusion of loss [detector efficiencies $\eta_a = \eta_b = \eta$ in Eq. (18)] for a FS-CS input $|\Psi_{\text{in}}\rangle_{ab} = |n\rangle_a |\beta = \sqrt{3}\rangle_b$ for a 50:50 BS with mean number of photons in the b mode $\bar{n}_b = |\beta|^2 = 3$: (a) and (b) $\eta = 1.0$, lossless, and (c) and (d) $\eta = 0.95$, 5% loss.

by $P_D(t|n') = \binom{n'}{t} \eta^t (1 - \eta)^{n'-t}$, which is again the same Bernoulli factor arising from the “fictitious BS” that was used in Eq. (17) to model loss. Therefore, the total probability of detecting t photons in the heralding arm of a single TMSS source is given [34] by

$$P_D^{\text{SPDC}}(t) = \sum_{n'=t}^{\infty} P_D(t|n') p_{n'}^{(\xi)} = \sum_{n'=t}^{\infty} \binom{n'}{t} \eta^t (1 - \eta)^{n'-t} p_{n'}^{(\xi)}, \quad (19)$$

which is the single-mode version of Eq. (18). For example, $P_D^{\text{SPDC}}(2)$ is the probability to detect two photons in the heralding arm of the TMSS source when n' are present, but $n' - 2$ have been lost (unregistered by the detector) and then summed over all possible values of $n' \geq 2$.

Ultimately, we are interested in the inverse conditional probability $P_{|n\rangle_{a'}}(n'|t)$ that given t photons were detected in the heralding arm (mode a'), these detections actually arose from the input state $|n'\rangle_{a'}$, implying that the output state in the heralded arm is $|n'\rangle_{b'}$. From the Bayes rule we have

$$P_{|n\rangle_{a'}}(n'|t) = \frac{P_D(t|n') p_{n'}^{(\xi)}}{P_D(t)} = \frac{P_D(t|n') p_{n'}^{(\xi)}}{\sum_{n''=t}^{\infty} P_D(t|n'') p_{n''}^{(\xi)}}, \quad (20)$$

where the numerator (denominator) in Eq. (20) is the summand (entire sum) in Eq. (19). In Fig. 12 we plot $P(n|n) \equiv P_{|n\rangle_{a'}}(n|t = n)$ as a function of detector efficiency η for $n \in \{1, 2, 3\}$.

As expected, $P(n|n)$ monotonically increases with η such that at perfect detection efficiency $\eta = 1$ for the number-resolving detector, it is certain that the n photons detected

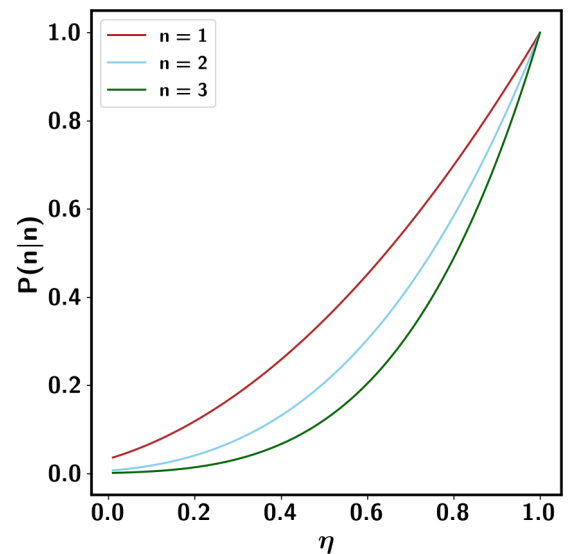


FIG. 12. Conditional probability $P(n|n) \equiv P_{|n\rangle_{a'}}(n|t = n)$ as a function of detector efficiency η for $n \in \{1, 2, 3\}$ that, given n photons were detected in the heralding arm (mode a') of the TMSS source, it arose from the state $|n\rangle_{a'}$.

arose from the input state $|n\rangle_{a'}$. As discussed above, state-of-the-art number-resolving TESs have efficiencies exceeding 87% [24]. This implies a probability of $P(2|2) = 0.71$ to detect the FS state $|2\rangle_{a'}$ from a strong TMSS source ($r = 1.5 \leftrightarrow -13$ dB of squeezing) at $\eta = 0.87$, resulting in the output state $|2\rangle_{b'} \rightarrow |2\rangle_a$ that can subsequently be mixed with the CS $|\beta\rangle_b$ to observe the CNLs and PNCs described above. For $|3\rangle_{b'} \rightarrow |3\rangle_a$ the probability drops to $P(3|3) = 0.63$ for the same values of r and η . Bright SPDC sources in combination with photon-number-resolving detectors have been used recently to experimentally realize multiphoton subtracted TMSSs by Magaña-Loaiza *et al.* (see Fig. 2 of [6]) up to ten photons, based on theoretical proposals of Carranza and Gerry [5].

Since the extended HOM effects discussed in this work, CNLs and PNCs, depend on the properties of the beam-splitter coefficients for nonclassical FS input states, it is natural to inquire if such analogous effects are also present for a collection of atoms. The answer is affirmative, and this analogy is discussed in Appendix D through the use of the Schwinger representation of $\text{su}(2)$ and the formal correspondence between a pair of dual-mode Fock basis states $|n, m\rangle_{ab}$ with angular momentum states $|J, M\rangle$ often used to describe a collection of atoms.

VI. CONCLUSION

In this work we have shown that the parity of a nonclassical state of light has a dominant influence on the interference effects at a beam splitter, irrespective of the state it is mixed with at the other input port. The parity of the nonclassical input carves deep valleys in the output joint number distribution. A limiting case of our analysis is the Hong-Ou-Mandel effect, but we found dramatic additional richness in the interferences beyond this. This counterintuitive influence of even a single photon to control the output of a beam splitter illuminated by any field, e.g., coherent or even a noisy thermal field, demonstrates the extraordinary power of nonclassicality. We explained the origin of these effects and explored prospects for observing them with currently available number-resolving detectors.

The extension of the HOM effect arises from the inherent filtering property of a 50:50 BS when acting on nonclassical states. We have shown that if the a mode of the BS contains only odd numbers of photons (an odd-parity state), a central nodal line exists for the output joint probability distribution $P(m_a, m_b, \theta = \pi/2)$ for measuring m_a photons in the a mode and m_b photons in the b mode, independently of the input state in the b mode, pure or mixed. In the simplest case of a single-photon FS-FS input state $|1, 1\rangle_{ab}$, this result reduces to the well-known Hong-Ou-Mandel effect for the destructive interference of the quantum amplitude for the output $|1, 1\rangle_{ab}$ state of a 50:50 BS. We have shown that this CNL results from the intrinsic property of the BS itself acting on nonclassical Fock states of odd number. This produces zeros in the angular portion of the beam-splitter coefficients which dictate the mixing of the nonclassical basis photon-pair FS $|n, m\rangle_{ab}$ (for which arbitrary a - and b -mode input states can be expanded) such that $m_a + m_b = n + m$.

We have further shown that for a 50:50 BS there always exists off-diagonal pseudonodal curves upon which numerous sets of noncontiguous zeros lie, which carve out valleys (local minima) in the output photon-number distribution. These PNCs lie symmetrically placed about the diagonal symmetry line $m_a = m_b$ of the output joint photon-number distribution and exist for any input FS $|n > 0\rangle_a$ entering the a mode, with n even or odd. For the case of a FS-CS input $|n\rangle_a |\beta\rangle_b$ we have provided explicit analytic solutions in parametric form $(m_a(k), m_b(k))$ in terms of another integer $k \in \mathbb{Z}$. That the results presented in this work are universal has been explicitly demonstrated for various combinations of odd-parity input states containing odd numbers of photons entering the a mode mixed with arbitrary states entering the b mode. In addition, we have explored the existence of the PNC for a BS of arbitrary reflectivity, in particular $\theta = \pi/3$, and shown that they must disappear as one approaches the extreme limits of 0 or 100% BS transmittance.

With today's state-of-the-art photon-number-resolving detectors (TESs) using principal component analysis to plot as a histogram the energy bins for a low number of photons (up to roughly 5 reliably, possibly 10–20 in some special cases, with high detection efficiencies), experiments to verify the predicted CNLs and PNCs should be experimentally feasible, even in the presence of a small amount of noise.

There is another feature of the output state joint photon-number distribution that was first highlighted in BMG's paper [15] (where the CNL was noted and briefly discussed) having to do with the relative heights of the constructive interference fringes appearing when mixing coherent light with increasing numbers of n photons. As evident from Figs. 2 and 3, increasing the number of photons in the Fock state initially occupying the a mode tends to push the peaks towards the two axes, creating a U-shaped distribution along the antidiagonal that becomes more pronounced as n is taken to be larger. This is similar to the familiar distribution one gets when mixing twin Fock states at a balanced beam splitter to produce the arc sine states [35,36]. Such a distribution, owing to its similarity to the well-known N00N state [37], has been known to be conducive to enhanced phase sensitivity beyond the standard quantum limit in interferometric measurements [38]. Further investigation of the structure of this antidiagonal U-shaped distribution in light of the extended HOM effect is left for future work.

As a potential application, the results obtained in this work can be used in quantum key distribution protocols. If Alice and Bob decide to exchange qubits using nonorthogonal quantum states with different parity (i.e., odd or even photon number), the ability to produce a joint photon distribution using number-resolving detectors can help detect the presence of an eavesdropper. In principle, when using multiphoton states, an eavesdropper can gain sufficient information by carrying out a photon-number-splitting attack through quantum non-demolition measurements. Eve separates the photons using an adjustable beam splitter, thereby sending a portion of the photons to Bob and storing the rest with her. However, because Bob only detects Eve by examining the detection rate, Eve's presence can go unnoticed unless he uses methods such as a decoy state technique to overcome a photon-number-splitting attack. However, investigating the photon statistics on his end

can be used to reveal the presence of Eve. Suppose Alice and Bob agree ahead of time that when they are ready to check for the presence of Eve, Alice will send a state of n photons. As described, the joint photon distribution will exhibit n PNCs if n is even and $n - 1$ PNCs plus one CNL if n is odd. If Eve collects some of the photons transmitted to Bob, the number of PNCs or PNCs and CNLs will change, revealing the presence of the eavesdropper. If Eve tries to detect photons and then transmit a copy, she will send an incorrect number of photons unless she has a perfect detector. This method requires that the same state must be transmitted enough times to build up the joint photon-number distribution.

Through the past three decades many researchers have hinted at the existence of features analogous to the CNL for special specific input state cases (typically involving a single photon in the a mode and some interesting state in the b mode). However, very little, if any, attention has been paid to the existence and origin of the PNC. This work represents a comprehensive amalgamation of such past observations, plus a systematic explanation for their occurrence, as an intrinsic property of the 50:50 BS itself acting on nonclassical states. Our results reduce to the well-known HOM effect in the limiting case of two single-photon inputs to the BS, and hence can be rightfully deemed a general extension of the HOM effect.

ACKNOWLEDGMENTS

P.M.A. would like to acknowledge support of this work from the Air Force Office of Scientific Research. R.J.B. would like to thank the National Academy of Sciences for support of this work through a National Research Council fellowship. C.C.G. would like to acknowledge support for this work provided by the Air Force Research Laboratory Visiting Faculty Fellowship Program under Grant No. FA8750-20-3-1003. The authors would like to thank M. L. Fanto and C. C. Tison for useful experimental discussions and considerations. Any opinions, findings, and conclusions or recommendations expressed in this material are those of the author(s) and do not necessarily reflect the views of Air Force Research Laboratory or the U.S. Navy.

APPENDIX A: ACTION OF THE BS ON $|n, m\rangle_{ab}$

We need to know how an ideal lossless BS acts on an arbitrary two-mode FS input basis state $|n, m\rangle_{ab}$ presented at its two input ports. Let us define the BS transformation (Hamiltonian) on two modes a and b as $B = (\theta/2)(ab^\dagger + a^\dagger b)$. Here $T \equiv \cos^2(\theta/2)$ is the BS transmissivity and $R = (1 - T) = \sin^2(\theta/2)$ is the BS reflectivity such that $R + T = 1$, as shown in Fig. 13. [Note that we call the quantities $\sin(\theta/2)$ and $\cos(\theta/2)$ reflection and transmission coefficients, respectively.] The factor of $1/2$ in the argument $\theta/2$ is introduced so that $\theta = \pi/2$ represents a 50:50 BS.

1. Conventions and operator transformations

The action of the BS on an arbitrary Fock pair basis state $|n\rangle_a |m\rangle_b \equiv \frac{(a^\dagger)^n (b^\dagger)^m}{\sqrt{n!} \sqrt{m!}} |0\rangle_a |0\rangle_b$ is straightforwardly computed (see Chap. 5 of [25]) by applying the BS transformation

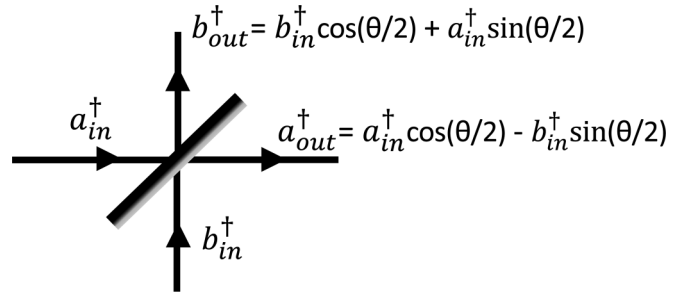


FIG. 13. Two optical modes a and b mixing on a BS of transmissivity $T = \cos^2(\theta/2)$. Here the bottom of the BS imparts a π phase shift of -1 upon reflection

to the last expression and expanding terms using the binomial theorem (since a^\dagger and b^\dagger commute).

Here we take the fundamental transformation of the annihilation operators by the unitary $U(\theta) \equiv U_{BS}(\theta)$ to be

$$\begin{aligned} \begin{bmatrix} a_{out} \\ b_{out} \end{bmatrix} &= U(\theta) \begin{bmatrix} a_{in} \\ b_{in} \end{bmatrix} U^\dagger(\theta) \\ &= \begin{bmatrix} \cos(\theta/2) & -\sin(\theta/2) \\ \sin(\theta/2) & \cos(\theta/2) \end{bmatrix} \begin{bmatrix} a_{in} \\ b_{in} \end{bmatrix} \equiv S_{BS}^T(\theta) \vec{a}_{in}, \quad (A1) \end{aligned}$$

where we have defined the matrix $S_{BS}^T(\theta)$ by the 2×2 rotation matrix in Eq. (A1).

Note that if we write the BS transformation S_{BS} of the out operators in terms of the in operators as $\vec{a}_{out}^\dagger = S_{BS}^T \vec{a}_{in}^\dagger$, then to transform an input state such as $|1\rangle_a |0\rangle_b = a_{in}^\dagger |0\rangle_a |0\rangle_b$, we need to write the in operators in terms of the out operators using the transpose transformation S_{BS} as $\vec{a}_{in}^\dagger = S_{BS} \vec{a}_{out}^\dagger$ [39] via

$$\vec{a}_{in}^\dagger = \begin{bmatrix} a_{in}^\dagger \\ b_{in}^\dagger \end{bmatrix} = \begin{bmatrix} \cos(\theta/2) & \sin(\theta/2) \\ -\sin(\theta/2) & \cos(\theta/2) \end{bmatrix} \begin{bmatrix} a_{out}^\dagger \\ b_{out}^\dagger \end{bmatrix} \equiv S_{BS} \vec{a}_{out}^\dagger \quad (A2)$$

$$\Rightarrow U(\theta) \vec{a}_{in}^\dagger U^\dagger(\theta) = S_{BS} \vec{a}_{out}^\dagger. \quad (A3)$$

We can now drop all the in and out labels and just remember to use the transformation S_{BS} when applying the BS transformation to creation operators when transforming from input states to output states, i.e.,

$$|\psi_{in}\rangle_{ab} \equiv f(\vec{a}^\dagger) |0\rangle_a |0\rangle_b \quad \text{for some function } f \text{ of } \vec{a}^\dagger = \begin{bmatrix} a^\dagger \\ b^\dagger \end{bmatrix} \quad (A4a)$$

$$\Rightarrow |\psi_{out}\rangle_{ab} = U(\theta) |\psi_{in}\rangle_{ab} \quad (A4b)$$

$$\begin{aligned} &= U(\theta) f(\vec{a}^\dagger) U^\dagger(\theta) U(\theta) |0\rangle_a |0\rangle_b \\ &= f(S_{BS} \vec{a}^\dagger) |0\rangle_a |0\rangle_b \quad \text{using } \vec{a}^\dagger \xrightarrow{U(\theta)} S_{BS} \vec{a}^\dagger, \quad (A4c) \end{aligned}$$

$$S_{BS} = \begin{bmatrix} \cos(\theta/2) & \sin(\theta/2) \\ -\sin(\theta/2) & \cos(\theta/2) \end{bmatrix}. \quad (A4d)$$

Equations (A4a), (A4b), and (A4d) are the primary BS operator transformation equations that we will employ throughout this work.

2. BS transformation of the state $|n, m\rangle_{ab}$ and examples

We are now interested in the BS transformed output state $|n, m\rangle_{ab}^{(\text{out})} = U(\theta)|n, m\rangle_{ab}$ when n photons are present at input mode a and m photons are present at input mode b . The derivation is easily carried out (see [25] and Sec. VI) with the results given below using S_{BS} to transform an input state $|n\rangle_a|m\rangle_b$ to an output state, yielding

$$|n, m\rangle_{ab} \rightarrow |n, m\rangle_{ab}^{(\text{out})} \equiv \sum_{p=0}^{n+m} f_p^{(n,m)} |p\rangle_a |n+m-p\rangle_b, \quad (\text{A5a})$$

$$f_p^{(n,m)} = \sum_{q=0}^n \sum_{q'=0}^m \delta_{p,q+q'} \binom{n}{q} \binom{m}{q'} \sqrt{\frac{p!(n+m-p)!}{n!m!}} \times (-1)^{q'} [\cos(\theta/2)]^{m+q-q'} [\sin(\theta/2)]^{n-q+q'} \quad (\text{A5b})$$

[40]. Note that the δ function $\delta_{p,q+q'}$ ensures that the BS mixes the original input state $|n\rangle_a|m\rangle_b$ only among the $n+m+1$ states of total photon number $n+m$ of the form $\{|0\rangle_a|n+m\rangle_b, |1\rangle_a|n+m-1\rangle_b, \dots, |n\rangle_a|m\rangle_b, \dots, |n+m-1\rangle_a|1\rangle_b, |n+m\rangle_a|0\rangle_b\}$. The (real) BS coefficients $f_p^{(n,m)}$ are easily worked out by hand by considering states $|n\rangle_a|m\rangle_b$ up to $n+m=2$ at the input ports of BS, as shown in Table I.

TABLE I. Beam-splitter coefficients $f_p^{(n,m)}(\theta)$ for fixed input numbers of photons: (a) $n+m=1$ and (b) $n+m=2$.

(a)			
f \ p	$f_p^{(0,1)}(\theta)$	$f_p^{(1,0)}(\theta)$	
0	$\cos(\theta/2)$	$\sin(\theta/2)$	
1	$-\sin(\theta/2)$	$\cos(\theta/2)$	
(b)			
f \ p	$f_p^{(0,2)}(\theta)$	$f_p^{(1,1)}(\theta)$	$f_p^{(2,0)}(\theta)$
0	$\cos^2(\theta/2)$	$\frac{1}{\sqrt{2}} \sin(\theta)$	$\sin^2(\theta/2)$
1	$-\frac{1}{\sqrt{2}} \sin(\theta)$	$\cos(\theta)$	$\frac{1}{\sqrt{2}} \sin(\theta)$
2	$\sin^2(\theta/2)$	$-\frac{1}{\sqrt{2}} \sin(\theta)$	$\cos^2(\theta/2)$

Note that for each (n, m) we have $\sum_{p=0}^{n+m} |f_p^{(n,m)}|^2 = 1$, which just indicates that the BS transformation is unitary. Note that the $f_p^{(n,m)}(\theta)$ are just the Wigner rotation coefficients for the representation of a system with spin $J = (n+m)/2$ in the angular momentum basis $|J, M\rangle$ with $2J+1 = n+m+1$ states $M \in \{-J, -J+1, \dots, J\}$, where $M(p) = -J + p(2J)/(n+m)$ for $p \in \{0, \dots, n+m\}$ (see also Appendixes A and B of [13]).

3. Derivation of the BS coefficients $f_p^{(n,m)}(\theta)$ [Eq. (A5b)] and their hyperbinomial form

The derivation of the BS coefficients $f_p^{(n,m)}(\theta)$ in Eq. (A5b) is a straightforward exercise (see [25], Chap. 5). Consider the dual Fock input state $|n\rangle_a|m\rangle_b$ entering the BS. Using the BS transformation rules and the binomial expansion, we have

$$\begin{aligned} |n\rangle_a|m\rangle_b &= \frac{(a^\dagger)^n (b^\dagger)^m}{\sqrt{n!} \sqrt{m!}} |0, 0\rangle_{ab} \xrightarrow{U(\theta)} \frac{[a^\dagger \cos(\theta) + b^\dagger \sin(\theta)]^n [b^\dagger \cos(\theta) - a^\dagger \sin(\theta)]^m}{\sqrt{n!} \sqrt{m!}} |0, 0\rangle_{ab} \\ &= \frac{1}{\sqrt{n!m!}} \sum_{q=0}^n \binom{n}{q} [\cos(\theta/2)a^\dagger]^q [\sin(\theta/2)b^\dagger]^{n-q} \sum_{q'=0}^m \binom{m}{q'} [\cos(\theta/2)b^\dagger]^{m-q'} [-\sin(\theta/2)a^\dagger]^{q'} |0, 0\rangle_{ab}, \\ &\equiv \sum_{p=0}^{n+m} f_p^{(n,m)} |p\rangle_a |n+m-p\rangle_b, \end{aligned} \quad (\text{A6a})$$

where we define

$$f_p^{(n,m)}(\theta) \equiv \sum_{q=0}^n \sum_{q'=0}^m \delta_{p,q+q'} \binom{n}{q} \binom{m}{q'} \sqrt{\frac{p!(n+m-p)!}{n!m!}} (-1)^{q'} [\cos(\theta/2)]^{m+(q-q')} [\sin(\theta/2)]^{n-(q-q')} \quad (\text{A6b})$$

$$= \sqrt{\frac{p!(n+m-p)!}{n!m!}} [\cos(\theta/2)]^{m-p} [\sin(\theta/2)]^{n+p} (-1)^p \sum_{q=0}^n \binom{n}{q} \binom{m}{p-q} \left(\frac{-1}{\tan^2(\theta/2)}\right)^q. \quad (\text{A6c})$$

Note that in Eq. (A6a) we have introduced the new summation variable $p \in \{0, n+m\}$ and the boundary condition that $p \equiv q+q'$ by including $\sum_{p=0}^{n+m} \delta_{p,q+q'}$ to ensure that the Fock states $|p\rangle_a$ and $|n+m-p\rangle_b$ stay in bounds. In Eq. (A6c) we have performed the sum over q' , yielding $q' = p-q$ [and noting that if the q index goes out of bounds we obtain 0 from the binomial coefficients, i.e., $\binom{m}{p-q} = 0$ for $p-q < 0$,

since $1/(-k)! = 0$ for integer $k \in \mathbb{Z}_{\geq 0}$], and then pull out all non- q -dependent terms from the sum over q .

We now put Eq. (A6c) in one last final hyperbinomial form, which will be beneficial when we compute probabilities of m_a and m_b photons in modes a and b , respectively. Let us consider the binomial term $\binom{m}{p-q} = \frac{m!}{(p-q)!(m-p+q)!} \equiv$

$\frac{m!}{(p-q)!(m+n-p)-(n-q)!}$ in the summation in Eq. (A6c). Now using the definition of the falling factorial $(x)_k = \frac{x!}{(x-k)!}$, we can replace the factorial terms in the denominator using $\frac{1}{(x-k)!} = \frac{(x)_k}{x!}$ so that $\binom{m}{p-q} = \frac{m!(p)_q(m+n-p)_{n-q}}{p!(m+n-p)!}$. In anticipation of measurement results to come, we also write $m! \equiv [(m +$

$n) - n]! = \frac{(m+n)!}{(m+n)_n}$. This yields the final desired form $\binom{m}{p-q} = \binom{m+n}{p} \frac{(p)_q(m+n-p)_{n-q}}{(m+n)_n}$. Finally, by multiplying the summand by $1 = \frac{\tan^{2n}(\theta/2)}{\tan^{2n}(\theta/2)}$ and pulling out all non- q terms from the summation, we can write Eq. (A6c) finally as

$$f_p^{(n,m)}(\theta) = \frac{(-1)^{p+n}}{\sqrt{n!(m+n)_n}} \sqrt{\binom{m+n}{p}} [\cos(\theta/2)]^{m-p} [\sin(\theta/2)]^{p-n} g_p^{(n,m)}(\theta), \quad (\text{A7a})$$

$$g_p^{(n,m)}(\theta) \equiv \sum_{q=0}^n \binom{n}{q} (-1)^q (p)_{n-q} [\cos^2(\theta/2)]^{n-q} (m+n-p)_q [\sin^2(\theta/2)]^q. \quad (\text{A7b})$$

We see that the zeros of $f_p^{(n,m)}(\theta)$ are governed by the summation over the q term $g_p^{(n,m)}(\theta)$ in Eq. (A7a).

Since the state exiting the BS with a dual FS input $|n, m\rangle_{ab}$ is given by $|n, m\rangle_{ab}^{(\text{out})} = \sum_{p=0}^{n+m} f_p^{(n,m)} |p\rangle_a |n+m-p\rangle_b$, the amplitude to be in the output state $|m_a, m_b\rangle_{ab}$ is given by ${}_{ab}\langle m_a, m_b | n, m\rangle_{ab}^{(\text{out})} = f_p^{(n,m)}(\theta) \delta_{p,m_a} \delta_{m,m_a+m_b-n}$. Note that the particular form of Eq. (A7b) was chosen in anticipation of the above δ functions which set $p \rightarrow m_a$ and $m+n-p \rightarrow (m_a+m_b-n) + n - m_a = m_b$. It is therefore useful to rewrite Eqs. (A7a) and (A7b) one final time in terms of the measured number of photons (m_a, m_b) at the output ports of the BS since the joint photon-number probability $P(m_a, m_b, \theta)$ is proportional to $[g_{p=m_a}^{(n,m=m_a,m_b)}(\theta)]^2 \equiv [g(m_a, m_b, \theta|n)]^2$. From Eqs. (A7a) and (A7b) we write the beam-splitter coefficient after measurement as

$$f_{p=m_a}^{(n,m=m_a+m_b-n)}(\theta) = \frac{(-1)^{m_a+n}}{\sqrt{n!(m_a+m_b)_n}} \sqrt{\binom{m_a+m_b}{m_a}} [\cos(\theta/2)]^{m_b-n} [\sin(\theta/2)]^{m_a-n} g_{p=m_a}^{(n,m_a+m_b-n)}(\theta), \quad (\text{A8a})$$

$$g_{p=m_a}^{(n,m=m_a,m_b)}(\theta) = \sum_{q=0}^n \binom{n}{q} (-1)^q (m_a)_{n-q} [\cos^2(\theta/2)]^{n-q} (m_b)_q [\sin^2(\theta/2)]^q \equiv g(m_a, m_b, \theta|n) \quad (\text{A8b})$$

$$\equiv (m_a)_n [\cos^2(\theta/2)]^n {}_2F_1(-m_b, -n; m_a+1-n; -\tan^2(\theta/2)). \quad (\text{A8c})$$

Equations (A8a) and (A8b) are the primary equations from which we deduce the main results of this work. Note that Eq. (A8c) defines the formal sum of Eq. (A8b) in terms of the hypergeometric function ${}_2F_1(a, b; c; z)$ with a and b negative integers, which is well defined (see [28]) but nonetheless not representable in any form of special function whose properties can be readily exploited, even at the 50:50 BS angle $\theta = \pi/2$. However, in practice we find Eq. (A8b) more useful and more intuitively appealing for deriving the results in this paper. The crucial property of Eq. (A8b) is that one can always factor $\cos(\theta)$ when n is odd. This nontrivial (and heretofore overlooked) property is not readily apparent from Eq. (A8c) and properties of the hypergeometric function ${}_2F_1$, since the

latter involves factors of $\cos^2(\theta/2)$ and $\tan^2(\theta/2)$ vs $\cos(\theta) = \cos^2(\theta/2) - \sin^2(\theta/2)$. Note that if n is odd, Eq. (A8b) contains an even number of terms, while if n is even the sum contains an odd number of terms. It is the particular nearly binomial form of Eq. (A8b), with even and odd numbers of terms, that has allowed us to deduce properties of FSs and hence superposition of FSs entering the ports of the BS.

APPENDIX B: PROOF OF Eq. (14a)

In this Appendix we prove that we can always factor out $\cos(\theta)$ from $g(m_a, m_b, \theta|n)$ when n is odd, which is the origin of the CNL in the extended HOM effect. From Eq. (A8b) we have

$$g(m_a, m_b, \theta|n) = \sum_{q=0}^n \binom{n}{q} (-1)^q (m_a)_{n-q} [\cos^2(\theta/2)]^{n-q} (m_b)_q [\sin^2(\theta/2)]^q \quad (\text{B1a})$$

$$\stackrel{m_a=m_b=m'}{\implies} g(m', m', \theta|n) = \sum_{q=0}^n \binom{n}{q} (-1)^q (m')_{n-q} (m')_q [\cos^2(\theta/2)]^{n-q} [\sin^2(\theta/2)]^q \quad (\text{B1b})$$

$$\equiv \sum_{q=0}^n \binom{n}{q} (-1)^q (m')_{n-q} (m')_q x^{n-q} y^q, \quad (\text{B1c})$$

where for convenience we have defined $x = \cos^2(\theta/2)$ and $y = \sin^2(\theta/2)$. The goal is to show that for n odd, one can always factor out $x - y = \cos^2(\theta/2) - \sin^2(\theta/2) = \cos(\theta) \xrightarrow{\theta=\pi/2} 0$ for a 50:50 BS [since the CNL is then given by $P(m', m', \theta|n) \propto g^2(m', m', \theta|n) \xrightarrow{\theta=\pi/2} 0$].

For n odd, there is an even number of terms in Eq. (B1c), the first $(n-1)/2$ of which have the same magnitude but opposite sign of the latter $(n-1)/2$ terms. This allows us to write

$$g(m', m', \theta|n) = \sum_{q=0}^{(n-1)/2} \binom{n}{q} (-1)^q (m')_{n-q} (m')_q [x^{n-q} y^q - x^q y^{n-q}] \quad (\text{B2a})$$

$$\equiv (x-y) \sum_{q=0}^{(n-1)/2} \binom{n}{q} (-1)^q (m')_{n-q} (m')_q x^q y^q \left[\sum_{k=1}^{n-2q} x^{(n-2q)-k} y^{k-1} \right], \quad (\text{B2b})$$

which is the proof of the main assertion. In moving from Eq. (B2a) to Eq. (B2b) we have used the algebraic identities that for fixed $q \in \{0, 1, \dots, (n-1)/2\}$ with n odd and for any integer r we have

$$\begin{aligned} x^{n-q} y^q - x^q y^{n-q} &= x^q y^q (x^{n-2q} - y^{n-2q}) \\ &= x^q y^q (x-y) \sum_{k=1}^{n-2q} x^{(n-2q)-k} y^{k-1}, \end{aligned} \quad (\text{B3a})$$

$$x^r - y^r = (x-y) \sum_{k=1}^r x^{r-k} y^{k-1}. \quad (\text{B3b})$$

Equation (B3b) follows simply by expanding the terms on the right-hand side and seeing that all terms cancel in pairs, except for the first and last unpaired terms x^r and $-y^r$. The first identity (B3a) is best illustrated by explicitly checking its validity on small values of n and then proving by induction. For example, using $n=5$, Eq. (B3a) yields

$$x^{n-q} y^q - x^q y^{n-q} \rightarrow n=5, \quad q \in \{0, 1, 2\}, \quad (\text{B4a})$$

$$x^5 - y^5 = x^0 y^0 (x^5 - y^5) \quad (\text{for } q=0) \quad (\text{B4b})$$

$$= (x-y)(x^4 + x^3 y + x^2 y^2 + x y^3 + y^4),$$

$$x^4 y - x y^4 = x^1 y^1 (x^3 - y^3) \quad (\text{for } q=1) \quad (\text{B4c})$$

$$= xy(x-y)(x^2 + xy + y^2),$$

$$x^3 y^2 - x^2 y^3 = x^2 y^2 (x^1 - y^1) \quad (\text{for } q=2), \quad (\text{B4d})$$

where we have made repeated use of Eq. (B3b). Thus, for each summand labeled by q above, one is able to factor out the term $(x-y)$. The general proof then follows by induction.

APPENDIX C: ANALYTIC POLYNOMIALS $m_a(k)$ AND $m_b(k)$ FOR PNC IN FIGS. 5 AND 7

In this Appendix we provide Tables II–IV, which list analytic results for zeros indicating complete destructive interference in the case of a non-50:50 beam splitter.

TABLE II. Polynomials $(m_a(k), m_b(k))$ (with $m_b \geq m_a$) that identically solve $g(m_a, m_b, \theta = \pi/2|n=2) = 0$ [see upper branch of Fig. 5(a)]. Lower branch solutions are given by the pairs $(m_b(k), m_a(k))$.

$(m_a(k), m_b(k))$
$(2k^2 - k, 2k^2 - 3k + 1)$
$(2k^2 + k, 2k^2 + 3k + 1)$
$(8k^2 + k, 8k^2 + 6k + 1)$
$(2k^2 - 5k + 3, 2k^2 - 3k + 1)$
$(2k^2 + 3k + 1, 2k^2 + 5k + 3)$
$(8k^2 + 6k + 1, 8k^2 + 10k + 3)$
$(2k^2 + 5k + 3, 2k^2 + 7k + 6)$
$(2k^2 + 7k + 6, 2k^2 + 9k + 10)$

TABLE III. Polynomials $(m_a(k), m_b(k))$ (with $m_b \geq m_a$) that identically solve $g(m_a, m_b, \theta = \pi/2|n=3) = 0$ (with CNL $m_a = m_b = k$) [see the upper branch of Fig. 5(b)]. Lower branch solutions are given by the pairs $(m_b(k), m_a(k))$.

$(m_a(k), m_b(k))$
(k, k)
$(6k^2 + 7k + 2, 6k^2 + 13k + 7)$
$(6k^2 + 5k + 1, 6k^2 + 11k + 5)$

TABLE IV. Polynomials $(m_a(k), m_b(k))$ that identically solve $g(m_a, m_b, \theta = \pi/3|n=2) = 0$. See the legends of Fig. 7.

$(m_a(k), m_b(k))$
$(12k^2 + k, 36k^2 - 9k)$
$(12k^2 + k, 36k^2 + 15k + 1)$
$(12k^2 + 7k + 1, 36k^2 + 9k)$
$(12k^2 + 7k + 1, 36k^2 + 33k + 7)$
$(12k^2 + 17k + 6, 36k^2 + 39k + 10)$
$(12k^2 + 23k + 11, 36k^2 + 57k + 22)$

APPENDIX D: THE HOM EFFECT AND THE ANALOGOUS CNL FOR ATOMIC SYSTEMS

The HOM effect depends upon the properties of the beam-splitter coefficients for nonclassical FS input states. Since these coefficients are essentially the components of the Wigner SU(2) rotation matrices [13], it is natural to ask if complete destructive interference of quantum amplitudes, as

well as features analogous to the CNL, also exists for collections of atoms. The answer is yes if one makes use of the formal correspondence of the Schwinger representation for $su(2)$ in terms of a pair of bosonic modes [41]

$$J_x = \frac{1}{2}(ab^\dagger + a^\dagger b), \quad (\text{D1a})$$

$$J_y = \frac{i}{2}(ab^\dagger - a^\dagger b), \quad (\text{D1b})$$

$$J_z = \frac{1}{2}(a^\dagger a + b^\dagger b), \quad (\text{D1c})$$

with commutators $[J_i, J_j] = \epsilon_{ijk} J_k$, $i \in \{1, 2, 3\} \leftrightarrow \{x, y, z\}$. In Eq. (D1a) [Eq. (D1b)], J_x (J_y) has the form of a BS transformation of unitary form $U(\theta) = e^{-iJ_x \theta}$ ($e^{-iJ_y \theta}$). Because of the use of the pseudo-angular-momentum formalism involved in the Schwinger representation, a two-mode photon state $|\Psi\rangle = \sum_{n,m=0}^{\infty} c_{n,m} |n, m\rangle_{ab}$ can also be written in the angular momentum form $|\Psi\rangle = \sum_{J=\{0,1/2,1,3/2,\dots\}} \sum_{M=-J}^J c_{J+M, J-M} |J, M\rangle_{ab}$ for angular momentum states $|J, M\rangle$ with angular momentum $J = (n+m)/2$ and spin projections $M = (n-m)/2 \in \{-J, -J+1, \dots, J\}$.

For N_A two-level atoms, the collective atomic spin operators $J_i = \frac{1}{2} \sum_{k=1}^{N_A} \sigma_i^{(k)}$ define the Dicke (pseudo-angular-momentum) states given by $|J, M\rangle$ with effective angular momentum $J = N_A/2$ and effective spin projections $M \in \{-J, -J+1, \dots, J\}$. The Dicke states $|J, M\rangle$ are defined in terms of the individual ground $|g\rangle$ and excited $|e\rangle$ atomic states as $|J, J\rangle = |e\rangle^{\otimes N_A=2J}$ (all atoms excited) and $|J, -J\rangle = |g\rangle^{\otimes N_A=2J}$ (all atoms in the ground state) with intermediate steps consisting of superpositions of $J+M$ atoms in the excited state and $J-M$ atoms in the ground state.

A general collective atomic (input) state (for a fixed number N_A of atoms) is given by $|\Psi_A\rangle = \sum_{M=-J}^J c_M |J, M\rangle$. The analogy of the 50:50 BS is the $\pi/2$ pulse of the Ramsey sequence acting on each angular momentum state

$$|J, M\rangle \xrightarrow{U_{\text{BS}}} |J, M\rangle^{(\text{out})} = e^{-iJ_x \theta} |J, M\rangle = \sum_{M'} |J, M'\rangle d_{M',M}^J(\theta) \quad (\text{D2})$$

for a general BS angle θ . Here the Wigner rotation matrices $d_{M',M}^J(\theta)$ are related to the BS coefficients $f_p^{(n,m)}(\theta)$ via

$$d_{p-(n+m)/2, (n-m)/2}^{(n+m)/2}(\theta) \equiv f_p^{(n,m)}(\theta). \quad (\text{D3})$$

We can express each angular momentum state in terms of a pair of dual (Schwinger) a and b number states (FSs) via

$$|J, M\rangle_{JM} \leftrightarrow |n = J + M, m = J - M\rangle_{ab}, \quad (\text{D4a})$$

$$|n, m\rangle_{ab} \leftrightarrow \left| J = \frac{n+m}{2}, M = \frac{n-m}{2} \right\rangle_{J,M}. \quad (\text{D4b})$$

Here $J+M$ is the number of atoms in their excited state and $J-M$ is the number of atoms in their ground state. In the above we have put the subscript JM on the atomic Dicke states to distinguish them from the a - and b -mode FSs.

With the above correspondences in hand, consider the general atomic input state for a fixed number of atoms $N_A = 2J$ given by $|\Psi_{\text{in}}\rangle_A = \sum_{n=0}^{2J} c_n |J, M = n - J\rangle_{JM} = \sum_{n=0}^{2J} c_n |n, m = 2J - n\rangle_{a,b}$, which is transformed by the

BS transformation $U(\theta) = e^{-iJ_x \theta}$ to $\sum_{n=0}^{2J} c_n |n, m = 2J - n\rangle_{a,b}^{(\text{out})} = \sum_{n=0}^{2J} \sum_{p=0}^{2J} c_n f_p^{(n, 2J-n)}(\theta) |p, 2J - p\rangle_{a,b}$. If we now project this onto the dual FS $|m_a, m_b\rangle_{ab}$, and consider only states with odd n , we formally have the output joint probability distribution

$$P(m_a, m_b, \theta) = \left| \sum_{n=0}^{2J} c_n f_p^{(n, 2J-n)}(\theta) \right|^2 \quad (\text{D5a})$$

$$\xrightarrow[\substack{m_a=m_b=m'=J \\ n \text{ odd}}]{m_a=m_b=m'=J} P(m', m', \theta) \\ = \left| \sum_{n(\text{odd})=0}^{2J} c_n f_J^{(n, 2J-n)}(\theta) \right|^2 \quad (\text{D5b})$$

$$= \cos^2(\theta) \left| \sum_{n(\text{odd})=0}^{2J} c_n \tilde{f}_J^{(n, 2J-n)}(\theta) \right|^2, \quad (\text{D5c})$$

where we have used $m_a + m_b = n + m = 2J$ in Eq. (D5a) and $m_a = m_b = m' = J$ in Eq. (D5b). Here the summation $\sum_{n(\text{odd})=0}^{2J}$ indicates a sum over odd $n \in \{1, 3, 5, \dots, n_{\text{odd}}^{(\text{max})}\}$, where $n_{\text{odd}}^{(\text{max})} = 2J - 1$ ($2J$) if J is an integer (half-integer). Finally, in Eq. (D5b) we have used $f_J^{(n, 2J-n)}(\theta) \equiv \cos(\theta) \tilde{f}_J^{(n, 2J-n)}(\theta)$ for each n odd [see Eq. (14a) and Appendix B]. Therefore, $P(m', m', \pi/2) = P(J, J, \pi/2) = 0$ for a 50:50 BS ($\theta = \pi/2$) regardless of the coefficients c_n , as long as n is odd.

Now the projection onto the dual FS $|m', m'\rangle_{ab} = |J = m', M = 0\rangle_{JM}$ is a projection onto the atomic state with equal numbers of atoms in the ground and excited states for a collection of $N_A = 2J = 2m'$ atoms. The state $|J, M = 0\rangle$ can only occur of course for integer $J \in \mathbb{Z}_{\geq 0}$. Equation (D5c) shows that the quantum amplitude for this state will suffer complete destructive interference for a 50:50 BS [$\cos(\pi/2) = 0$] and hence will not be present in the output state (the HOM effect). For half-integer values of J there is simply never the possibility of an output state from the BS of equal numbers of atoms in both their excited and ground states [see the similar discussion after Eq. (14b) for photons], and hence no quantum interference effect is taking place.

With respect to the concept of the CNL (as in the photonic case), we will also find that for $\tilde{m} \neq m'$, $P(\tilde{m}, \tilde{m}, \pi/2) = 0$, but this will now entail having to make a measurement on a new number of atoms given by $\tilde{N}_A = 2\tilde{J} = 2\tilde{m} \neq N_A$. This means that the atomic ‘‘CNL’’ is spread out over a collection of measurements of experiments involving a different number of atoms for each diagonal element of the output probability distribution $P(m', m', \pi/2) = P(J, J, \pi/2)$, i.e., it is not a contiguous set of zeros representing complete destructive interference for a single collection of atoms N_A . However, for a given fixed number of atoms $N_A = 2J$, with input states of the form $\sum_{n(\text{odd})=0}^{2J} c_n |J, M = n - J\rangle_{JM}$, we have $P(J, J, \pi/2) = 0$, which is the extended HOM effect. Once again [see the discussion after Eq. (14b)] half the points in the atomic CNL (spread out over a different number of atoms $N_A = 2J$) are trivially zero, since the state $|J, M = 0\rangle$ is simply not capable of being present in the output (for J a half-integer), while the other half of points (for J an integer)

correspond to diagonal output states that have coefficients proportional to $\cos(\theta) \xrightarrow{\theta=\pi/2} 0$ for a 50:50 BS, which is the extended HOM effect of complete destructive interference of the output amplitude for the state $|J, M = 0\rangle$ (i.e., equal numbers

of atoms in the excited and ground states). This is the atomic analog of the CNL in the photonic case where the extended HOM effect occurs on output states $|m' = (n + m)/2, m'\rangle_{ab}$ with equal number of photons in each mode.

- [1] M. S. Kim, W. Son, V. Bužek, and P. L. Knight, Entanglement by a beam splitter: Nonclassicality as a prerequisite for entanglement, *Phys. Rev. A* **65**, 032323 (2002).
- [2] Z. Y. J. Ou, *Multi-Photon Quantum Interference* (Springer, New York, 2007).
- [3] J.-W. Pan, Z.-B. Chen, C.-Y. Lu, H. Weinfurter, A. Zeilinger, and M. Żukowski, Multiphoton entanglement and interferometry, *Rev. Mod. Phys.* **84**, 777 (2012).
- [4] M. Dakna, T. Anhut, T. Opatrny, L. Knöll, and D.-G. Welsch, Generating Schrödinger cat-like states by means of conditional measurements of a beam splitter, *Phys. Rev. A* **55**, 3184 (1997).
- [5] R. Carranza and C. C. Gerry, Photon-subtracted two-mode squeezed vacuum states and applications to quantum optical interferometry, *J. Opt. Soc. Am. B* **29**, 2581 (2012).
- [6] O. S. Magaña-Loaiza, R. d. J. León-Montiel, A. Perez-Leija, A. B. U'Ren, C. You, K. Busch, A. E. Lita, S. W. Nam, R. P. Mirin, and T. Gerrits, Multiphoton quantum-state engineering using conditional measurements, *npj Quantum Inf.* **5**, 80 (2019).
- [7] M. Dakna, L. Knöll, and D. G. Welsh, Photon-added state preparation via conditional measurement on a beam splitter, *Opt. Commun.* **145**, 309 (1998).
- [8] A. I. Lvovsky and J. Mlynek, Quantum-Optical Catalysis: Generating Nonclassical States of Light by Means of Linear Optics, *Phys. Rev. Lett.* **88**, 250401 (2002).
- [9] T. J. Bartley, G. Donati, J. B. Spring, X.-J. Min, M. Barbieri, A. Datta, B. J. Smith, and I. A. Walmsley, Multiphoton state engineering by heralded interference between single photons and coherent states, *Phys. Rev. A* **86**, 043820 (2012).
- [10] R. Birrittella, M. El-Baz, and C. C. Gerry, Photon catalysis and quantum state engineering, *J. Opt. Soc. Am. B* **35**, 1514 (2018).
- [11] R. Glauber, Letter to the editor, *Am. J. Phys.* **63**, 12 (1995).
- [12] C. K. Hong, Z. Y. Ou, and L. Mandel, Measurement of Subpicosecond Time Intervals between two Photons by Interference, *Phys. Rev. Lett.* **59**, 2044 (1987).
- [13] R. J. Birrittella, P. M. Alsing, and C. C. Gerry, The parity operator: Applications in quantum metrology, *AVS Quantum Sci.* **3**, 014701 (2021).
- [14] Formally, a quantum state of definite parity is a ± 1 eigenstate of the parity operator $(-1)^{a^\dagger a}$ [13]. Hence an odd- (even-)parity state is composed of only odd (even) numbers of photons.
- [15] R. Birrittella, J. Mimih, and C. C. Gerry, Multiphoton quantum interference at a beam splitter and the approach to Heisenberg-limited interferometry, *Phys. Rev. A* **86**, 063828 (2012).
- [16] F. Bouchard, A. Sit, Y. Zhang, R. Fickler, F. M. Miatto, Y. Yao, F. Sciarrino, and E. Karimi, Two-photon interference: The Hong-Ou-Mandel effect, *Rep. Prog. Phys.* **84**, 012402 (2021).
- [17] Z. Y. Ou, Quantum multiparticle interference due to a single photon, *Quantum Semiclass. Opt.* **8**, 315 (1996).
- [18] A. Kuzmich, D. Branning, L. Mandel, and I. A. Walmsley, Multiphoton interference effects at a beam splitter, *J. Mod. Opt.* **45**, 2233 (1998).
- [19] J. G. Rarity, P. R. Tapster, and R. Loudon, Non-classical interference between independent sources, *J. Opt. B: Quantum Semiclass. Opt.* **7**, S171 (2005).
- [20] S. A. Podoshvedov and N. B. An, Heralded hybrid CV-DV entanglement generation by quantum interference between CV state and DV delocalized photon, [arXiv:2101.02117](https://arxiv.org/abs/2101.02117).
- [21] W. K. Lai, V. Bužek, and P. L. Knight, Nonclassical fields in a linear directional coupler, *Phys. Rev. A* **43**, 6323 (1991).
- [22] K. Laiho, M. Schmidt, H. Suchomel, M. Kamp, S. Höfling, C. Schneider, J. Beyer, G. Weihs, and S. Reitzenstein, Photon-number parity of heralded single photons from a Bragg-reflection waveguide reconstructed loss-tolerantly via moment generating function, *New J. Phys.* **21**, 103025 (2019).
- [23] T. Gerrits, A. Lita, B. Calkins, and S. W. Nam, in *Superconducting Devices in Quantum Optics*, edited by R. H. Hadfield and G. Johansson, Quantum Science and Technology (Springer Nature, Cham, 2016), Chap. 2, pp. 31–60.
- [24] M. Schmidt, M. von Helversen, M. Lopez, F. Gericke, E. Schlottmann, T. Heindel, S. Kück, S. Reitzenstein, and J. Beyer, Photon-number-resolving transition-edge sensors for the metrology of quantum light sources, *J. Low Temp. Phys.* **193**, 1243 (2018).
- [25] G. S. Agarwal, *Quantum Optics* (Cambridge University Press, Cambridge, 2013).
- [26] C. C. Gerry and P. L. Knight, *Introductory Quantum Optics* (Cambridge University Press, Cambridge, 2004).
- [27] We note that the symbol $(x)_k$ is often used in the literature (see, e.g., [28]) to denote the rising or ascending factorial function or Pochhammer symbol $(x)_k \rightarrow x^{(n)} = (x+0)(x+1)(x+2)\cdots[x+(n-1)] = \frac{\Gamma(x+k)}{\Gamma(x)}$, $x^{(0)} \equiv 1$, $x^{(1)} = x$, $x^{(2)} = x(x+1)$, etc. In this work we employ the symbol $(x)_k$ for the descending factorial function and $(x)^k$ for the ascending factorial function.
- [28] M. Abramowitz and I. A. Stegun, *Handbook of Mathematical Functions* (Dover, New York, 1972), Eq. (6.1.22).
- [29] Reduce is *Mathematica*'s routine to solve Diophantine equations. It should be noted that it does not return all solutions, and for the case of a 50:50 BS it only returned the lower branch solutions of $g(m_a, m_b, \theta = \pi/2 | n = 2, 3) = 0$ in Figs. 5 and 7(a). For potential solutions to $g(m_a, m_b, \theta = \pi/3 | n = 3) = 0$ (Fig. 8), Reduce returned nonpolynomial solutions as roots of cubic equations $m_b = m_b(m_a)$.
- [30] S. M. Barnett, J. Jeffers, A. Gatti, and R. Loudon, Quantum optics of lossy beam splitters, *Phys. Rev. A* **57**, 2134 (1998).
- [31] P. M. Alsing, E. E. Hach, III, C. C. Tison, and A. M. Smith, A quantum optical description of losses in ring resonators based on field operator transformations, *Phys. Rev. A* **95**, 053828 (2017).
- [32] C. M. Nunn, J. D. Franson, and T. B. Pittman, Heralding on the detection of zero photons, *Phys. Rev. A* **104**, 033717 (2021).

- [33] D. F. Walls and G. J. Milburn, *Quantum Optics* (Springer, New York, 1994), Chap. 7.
- [34] K. R. Motes, J. P. Dowling, and P. P. Rohde, Spontaneous parametric down-conversion photon sources are scalable in the asymptotic limit for Boson sampling, *Phys. Rev. A* **88**, 063822 (2013).
- [35] R. A. Campos, B. E. A. Saleh, and M. C. Teich, Quantum-mechanical lossless beam splitter: SU(2) symmetry and photon statistics, *Phys. Rev. A* **40**, 1371 (1989).
- [36] C. C. Gerry and J. Mimih, The parity operator in quantum optical metrology, *Contemp. Phys.* **51**, 497 (2010).
- [37] J. P. Dowling, Quantum optical metrology the lowdown on high N00N states, *Contemp. Phys.* **49**, 125 (2008).
- [38] R. A. Campos, C. C. Gerry, and A. Benmoussa, Optical interferometry at the Heisenberg limit with twin Fock states and parity measurements, *Phys. Rev. A* **68**, 023810 (2003).
- [39] J. Skaar, J. C. G. Escartin, and H. Landro, Quantum mechanical description of linear optics, *Am. J. Phys.* **72**, 1385 (2004).
- [40] Note that Agarwal uses $S_{BS} = \begin{bmatrix} \cos(\theta) & i \sin(\theta) \\ i \sin(\theta) & \cos(\theta) \end{bmatrix}$, which results in $\cos(\theta/2) \rightarrow \cos(\theta)$, $\sin(\theta/2) \rightarrow i \sin(\theta)$, and the absence of the factor of $(-1)^{q'}$ in Eq. (A5b). The crucial minus signs in $g(m_a, m_b, \theta)$ then appear from factors of (i^2) raised to various powers.
- [41] B. Yurke, S. L. McCall, and J. R. Klauder, SU(2) and SU(1,1) interferometers, *Phys. Rev. A* **33**, 4033 (1986).